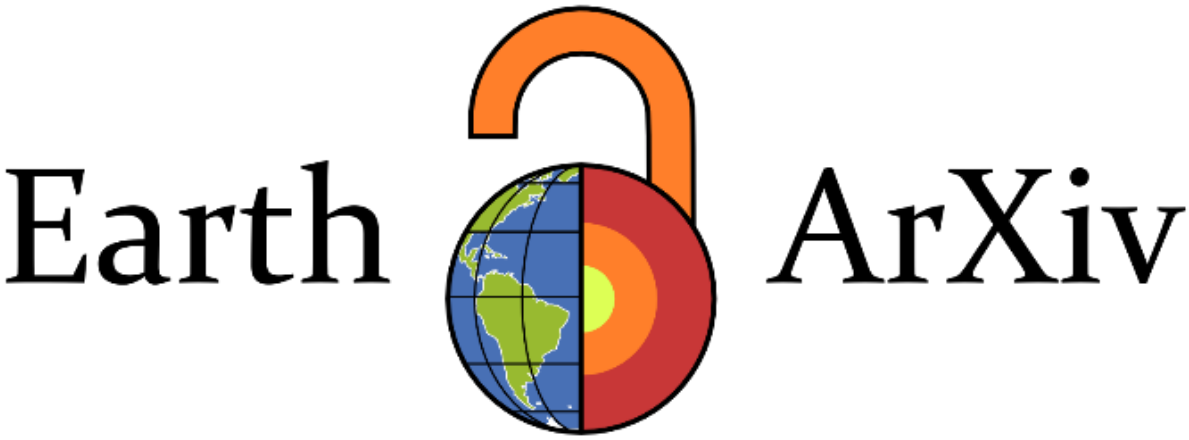

Anthropogenic acceleration of the leaky nitrogen cycle across the global land-river continuum

Minna Ma[1], Nicolas Vuichard[2], Haicheng Zhang[3], Tao Huang[4,5], Pierre Regnier[1]

[1] Department Geoscience, Environment and Society-BGEOSYS, Université libre de Bruxelles, 1050 Brussels, Belgium

[2] Laboratoire des Sciences du Climat et de l'Environnement, IPSL-LSCE CEA/CNRS/UVSQ, Orme des Merisiers, 91191, Gif-sur-Yvette, France

[3] School of Geography and Planning, Sun Yat-sen University, Guangzhou, Guangdong, 510006, China

[4] State Key Laboratory of Climate System Prediction and Risk Management, Nanjing Normal University, Nanjing 210023, PR China

[5] School of Geography Science, Nanjing Normal University, Nanjing 210023, China

Corresponding Author: minna.ma@ulb.be , Minna Ma

Abstract.

Lateral nitrogen transfer (LNT) along the land-river continuum plays a critical role in regulating global nitrogen (N) cycling and its feedbacks to climate, yet it remains poorly represented in land surface models. Here, we incorporate LNT into a global land surface model within an Earth System Model framework, enabling a process-based quantification of N transport, transformation, and associated riverine N_2O emissions at the global scale. The upgraded model, ORCHIDEE3-N_{lat}, captures the magnitude and broad spatial patterns of riverine N fluxes and N_2O emissions across major global river basins. Simulations for 1901–2020 indicate a strong anthropogenic intensification of LNT, with global dissolved inorganic nitrogen (DIN) delivery to rivers and export to the ocean increasing by ~245% and ~151%, respectively, while dissolved organic nitrogen (DON) shows more moderate increases (~32–38%), indicating a shift toward inorganic N dominance in aquatic systems. Riverine N_2O emissions increased substantially, accelerating after the 1960s and forming hotspots in intensively managed subtropical regions. Attribution analyses reveal different controls on N forms: global DIN increases were initially driven by sewage and atmospheric deposition, with fertilizer inputs becoming dominant after the 1960s, whereas DON dynamics were primarily governed by manure inputs and hydroclimatic variability. Attribution patterns vary markedly among continents, with Europe being the only region showing declines in lateral N fluxes and riverine N_2O emissions after the 1980s. Overall, anthropogenic perturbations more than doubled terrestrial N inputs, boosting riverine export and tripling riverine N_2O emissions—far outpacing changes over land, where terrestrial N_2O emissions increased by only ~25%. Despite a dramatic increase in global N export, the fraction of terrestrial N inputs reaching the ocean has decreased from 27% to 18% over the historical period, indicating reduced land-ocean connectivity and an intensified filtering role of the global river network.

Key words: lateral nitrogen transfer, riverine N_2O emissions, nitrogen export to the ocean, land-river continuum, land surface modelling, anthropogenic perturbations

1. Introduction

Reactive nitrogen (Nr), encompassing all biologically, chemically and radiatively active nitrogen (N) species except atmospheric N_2, is transformed through a complex network of processes that sustain a highly dynamic N cycle (Gruber & Galloway, 2008). This cycle strongly interacts with the Earth's climate system. For example, nitrous oxide (N_2O), a potent greenhouse gas (GHG), has a global warming potential about 300 times that of CO_2 on a per-

molecule basis and also contributes to stratospheric ozone depletion (Ravishankara et al., 2009). Moreover, the N cycle influences the carbon (C) cycle by regulating primary production and microbial activity in terrestrial, freshwater, and marine ecosystems, thereby indirectly affecting CO_2 and CH_4 fluxes and climate change (Morée et al., 2013; Seiler et al., 2024; Thornton et al., 2007; Zaehle et al., 2014).

Over the past century, human activities have dramatically accelerated the global N cycle (Fowler et al., 2013; Gruber & Galloway, 2008; Zhu et al., 2025), primarily through synthetic fertilizer production, fossil fuel combustion, and intensive animal husbandry (Erisman et al., 2008). In terrestrial ecosystems, increased inputs of Nr generally enhance soil N availability and plant productivity in N-limited systems. However, they also simulate soil microbial activity, accelerate nitrification and denitrification, increase emissions of nitrogenous gases such as NH_3, NO, and N_2O, and reduce ecosystem N retention efficiency under high or chronic Nr loading (Seiler et al., 2024; Thornton et al., 2007; Zaehle et al., 2014). As anthropogenic Nr is leached into rivers, aquatic primary production, organic matter decomposition, nitrification, and denitrification are stimulated, thereby strengthening coupled C–N cycling and increasing N_2O outgassing from aquatic systems (Beaulieu et al., 2011; Seiler et al., 2024; Maavara et al., 2019). Concurrently, the chemical composition of riverine dissolved Nr has been profoundly altered, shifting from diverse forms prior to human perturbation to a clear dominance of inorganic species under persistent anthropogenic nutrient enrichment (Wymore et al., 2021). These alterations result in widespread environmental impacts, including water quality degradation, eutrophication, hypoxia, biodiversity loss, and harmful algal blooms (Baron et al., 2013; Compton et al., 2011; Diaz & Rosenberg, 2008; Galloway, 2003).

The seminal work by Gruber and Galloway (2008) provides an Earth-system perspective on anthropogenic perturbations to the global Nr cycle, but does not explicitly resolve temporal trends, large-scale spatial variability, or process-level feedbacks, particularly along global river networks. As a critical linkage between terrestrial and marine Nr cycles, lateral Nr transfers along rivers remain insufficiently constrained, introducing substantial uncertainties in global N and C budgets (Battin et al., 2023; Billen et al., 2013; Galloway, 2003; Maranger et al., 2018). Explicit representation of riverine Nr processes is therefore essential for dynamically coupling land and ocean biogeochemical models, the land to ocean route being a preferential pathway through which anthropogenic perturbations on land propagate into the marine environment (Boyer et al., 2006; Tivig et al., 2021). Diagnosing ecosystem responses to anthropogenic perturbations therefore requires an Earth-system perspective (Gruber &

Galloway, 2008; Regnier et al., 2022). Such an Earth-system perspective is also required to assess greenhouse gas budgets, particularly N_2O emissions, a significant fraction of which is driven by the leaching of anthropogenic Nr from land (Suntharalingam et al., 2012, 2019; Yao et al., 2020).

Global riverine N_2O emissions have been simulated using a range of models that differ in process representation, spatial resolution and span, and temporal dynamics. Empirical approaches relate DIN loads to N_2O fluxes using statistical relationships or emission factors, providing early global estimates but lacking mechanistic detail (Hu et al., 2016; Kroeze et al., 2005). Process-based river-network models explicitly simulate nitrification–denitrification processes and their hydrological and geomorphic controls, enabling mechanistic interpretation of N_2O production in rivers (Beaulieu et al., 2011; Maavara et al., 2019; Marzadri et al., 2021, 2022). These models have improved previous estimates by assimilating observations through machine-learning techniques (Marzadri et al., 2021) or by applying stochastic approaches to assess uncertainties (Maavara et al., 2019; Lauerwald et al., 2019), but remain uncoupled from terrestrial ecosystem dynamics. Dynamic Land Ecosystem Model (DLEM) has integrated terrestrial and aquatic biogeochemical processes and simulated multi-decadal response of riverine N_2O emissions to anthropogenic N inputs and climatic forcing (Yao et al., 2020). However, the effects of land-use change and urban ecosystems on historical riverine N_2O emissions remain insufficiently represented.

Global nutrient models have also been developed to quantify N exports from land to rivers and the ocean. The Global Nutrient Export from Watersheds (GlobalNEWS) framework estimates riverine N export to the ocean as a function of catchment N inputs using highly simplified empirical representations of transport and in-stream processes (Mayorga et al., 2010; Seitzinger et al., 2005, 2010). The Integrated Model to Assess the Global Environment–Global Nutrient Model (IMAGE-GNM) couples hydrology with N delivery, transport, and retention across inland waters using a process-based representation, but lack a fully coupled terrestrial–aquatic N cycle. Similarly, Ma et al. (2025) developed a global lateral N transfer model (LSM_Nlateral_off) that resolves the hydrology as well as Nr transport and transformations along the global river network, enabling reconstruction and projection of lateral Nr fluxes under diverse anthropogenic drivers while capturing seasonal variability. However, the model operates offline, relying on prescribed terrestrial Nr inputs rather than a configuration in which terrestrial and aquatic Nr and C cycles and their feedbacks evolve synchronously. Coupled land–inland water models such as DLEM and LM3-based frameworks provide advanced

representations of Nr cycling within an integrated land-inland water framework (Lee et al., 2019, 2024a, 2024b; Tian et al., 2018; Yang et al., 2015). However, published estimates of lateral Nr transport from DLEM are currently limited to North America. Recent developments in the LM3 framework enable global-scale estimates and future projections (Lee et al., 2024b). Nevertheless, a systematic attribution of lateral Nr fluxes and their feedbacks to climate change and anthropogenic perturbations across the coupled land-river continuum remains unresolved.

Diverse modelling approaches and uneven observational constraints have led to diverging global estimates in both riverine N_2O emissions and Nr lateral fluxes. As recently synthesized by the Global Carbon Project through its Global Nitrous Oxide Budget, global riverine N_2O emissions fall within the 0.31-0.44 Tg N yr^{-1} range for present-day conditions (Tian et al., 2024). Model simulations over the past century suggest decadal growth rates on the order of 10%–20% (Wang et al., 2023; Yao et al., 2020). As already pointed out in the last assessment report by the IPCC (Canadell et al., 2021), this recently reported range is significantly lower than the values (1.05 Tg N yr^{-1}) reported in the pioneering studies by e.g., Seitzinger and Kroeze (1999). For Nr lateral transfers, values are mostly reported for the exports to the oceans and span the 35–49 Tg N yr^{-1} range for the contemporary period (Boyer et al., 2006; Green et al., 2004; Lee et al., 2024a; Mayorga et al., 2010; Vilmin et al., 2018). Ma et al (2025) also highlighted that discrepancies are larger at continental and watershed scales, sometimes exceeding 150 % for large river basins such as the Amazon, and the Ganges basin. This comparison among previous estimates thus highlights that land-to-ocean Nr exports and riverine N_2O emissions still face substantial uncertainties, which likely increase with spatial disaggregation. Model ensemble assessments regarding trends in lateral Nr fluxes and N_2O emissions are also critically missing. Furthermore, attribution of temporal changes to the wide diversity of direct (fertilizer, manure, etc…) and indirect (climate change, atmospheric composition) anthropogenic perturbations requires a holistic representation of the Nr cycle (Gruber and Galloway, 2008).

To achieve this aim, we develop ORCHIDEE3-N_{lat}, a land surface scheme within the IPSL Earth System Model (Boucher et al., 2020), which is enabled for lateral Nr transfer and N_2O emissions along the global river network. This integration provides a prognostic, process-based simulation framework for the co-evolution of land-river Nr dynamics. We first evaluate ORCHIDEE3-N_{lat} using observation-derived fluxes and concentrations of riverine NH_4^+, NO_3^- and DON, as well as N_2O emission rates. We then reconstruct the spatiotemporal dynamics of lateral Nr transfers and riverine N_2O emissions over the historical period (1901–2020), and

perform factorial simulations to attribute changes to natural and anthropogenic drivers operating on both terrestrial and aquatic systems. Finally, we propose a new global budget for the land-river Nr cycle that decomposes Nr fluxes into natural and anthropogenic components. Within this framework, we also aim to characterise the interannual and spatial variability of lateral Nr fluxes and riverine N_2O emissions, and identify the mechanisms governing their long-term changes over 1901–2020.

2. Methodology

2.1. Model description

ORCHIDEE3 is a global scale model coupling energy, water, C and N cycles in terrestrial ecosystems (Krinner et al., 2005; Vuichard et al., 2019). The representation of C and N cycles across the soil-plant-atmosphere system are based on the OCN model (Zaehle, 2013; Zaehle & Friend, 2010). With respect to soil N processes, nitrification and denitrification are simulated according to the DNDC (DeNitrification-DeComposition) model (Li et al., 1992, 2000; Zhang et al., 2002), tracking fluxes among soil ammonia/ammonium (NH_3/NH_4^+), NO_3^-, nitrogen oxides (NO_x), N_2O pools, and the atmosphere. In addition to vertical gaseous losses (NH_3, NO_x, N_2O and N_2), N is also delivered laterally via runoff and drainage into rivers. The representation of these lateral N fluxes and their fate within the global river network have been implemented in LSM_Nlateral_off (Ma et al., 2025) using outputs from ORCHIDEE-CNP (Goll et al., 2017, 2018; Sun et al., 2021) and ORCHIDEE-$C_{lateral}$ (Lauerwald et al., 2017; Zhang et al., 2022). Here we embed LSM_Nlateral_Off into ORCHIDEE3 to simulate the dissolved N (NH_4^+, NO_3^- and DON) cycles in terrestrial ecosystems and river networks, yielding ORCHIDEE3-N_{lat}.

ORCHIDEE3 simulates runoff, drainage, and associated inorganic N losses, which provide direct inputs to the lateral N transfer module. However, soil dissolved organic C (DOC) and dissolved organic N (DON) processes are not implemented in ORCHIDEE3. Therefore, in ORCHIDEE3-N_{lat} DOC leaching is simulated using an empirical formulation (Eq. S1) based on soil C content, runoff, drainage and soil temperature. DON leaching is then derived by applying observed C:N ratios of dissolved organic matter (ranging from 8 to 25, with a mean value of ~12) (Lutz et al., 2011; Maranger et al., 2018; Rodríguez-Cardona et al., 2022; Tipping et al., 2016). Consequently, factors that directly or indirectly influence soil organic C (SOC), runoff, drainage and soil temperature, for example climate change and inorganic N addition (synthetic fertilizer and atmospheric N deposition), can affect DON leaching and thereby alter the DON fluxes into rivers and their export to the ocean.

In the routing scheme of ORCHIDEE3-N_{lat} (Fig. 1), surface runoff (F_{RO}) feeds into the "fast" water reservoir (S_{fast_H2O}), while belowground drainage (F_{DR}) feeds into the "slow" water reservoir (S_{slow_H2O}). The outflows from these two reservoirs then feed into the "stream" water reservoir (S_{stream_H2O}). Water in the stream reservoir of a given grid cell is routed downstream ($F_{down2riv}$) into the stream reservoir of the adjacent downstream grid cell. The outflow rates from the fast ($F_{fastout\_H2O}$), slow ($F_{slowout\_H2O}$) and stream reservoirs ($F_{streamout\_H2O}$, F_{up2riv}, and $F_{down2riv}$) are calculated based on a reservoir-specific water residence time τ and a grid-cell-specific topographic index (f_{topo}; unitless; Table 1; Vörösmarty et al., 2000), which modulates τ to derive a water residence time for each reservoir attached to each river segment. Detailed formulations are provided in Ma et al. (2025).

Following the routing scheme of water, dissolved N contained in surface runoff and belowground drainage flows into the fast and slow reservoirs, respectively. Within these reservoirs, DON is decomposed into DIN, which undergoes transformations and losses via nitrification and denitrification (see below). The remaining fractions are transferred to the stream reservoir, which also receives point inputs from urban ecosystems via sewage (Fig. 1). In the stream reservoir, N continues to be transformed by the same biogeochemical reactions and is advected downstream from one grid cell to another along the river network.

A detailed description of N transfers and transformations within the river network can be found in Ma et al. (2025). Two main differences exist between LSM_Nlateral_off and the N routing module of ORCHIDEE3-N_{lat}. First, ORCHIDEE3-N_{lat} does not represent erosion of particulate (PON) and subsequent lateral transfer processes, as the sediment-erosion submodule that drives PON export is not currently integrated. Second, LSM_Nlateral_off treated DIN as a single pool and simulated only denitrification, whereas ORCHIDEE3-N_{lat} explicitly distinguishes NH_4^+ and NO_3^-, thereby including nitrification and denitrification along the routing pathway, as well as riverine N_2O emissions. Here, we mainly describe the newly added processes in ORCHIDEE3-N_{lat}, such as nitrification and N_2O emissions, as well as the dynamics of the related N species (i.e., NH_4^+, NO_3^-, N_2O). Specifically, the dynamics of NH_4^+ and NO_3^- in rivers are computed as follows:

$$\frac{dS_{fast\_NH4}}{dt} = F_{RO\_NH4} - F_{fastout\_NH4} + R_{fast\_DON} - R_{fast\_NIT} \quad (1)$$

$$\frac{dS_{slow\_NH4}}{dt} = F_{DR\_NH4} - F_{slowout\_NH4} + R_{slow\_DON} - R_{slow\_NIT} \quad (2)$$

$$\frac{dS_{stream\_NH4}}{dt} = F_{fastout\_NH4} + F_{slowout\_NH4} + F_{upstream\_NH4} + F_{sewage\_NH4} - F_{downstream\_NH4} + R_{stream\_DON} - R_{stream\_NIT} \quad (3)$$

$$\frac{dS_{fast\_NO3}}{dt} = F_{RO\_NO3} - F_{fastout\_NO3} + (1 - f_{NIT}) \times R_{fast\_NIT} - R_{fast\_DENIT} \quad (4)$$

$$\frac{dS_{slow\_NO3}}{dt} = F_{DR\_NO3} - F_{slowout\_NO3} + (1 - f_{NIT}) \times R_{slow\_NIT} - R_{slow\_DENIT} \quad (5)$$

$$\frac{dS_{stream\_NO3}}{dt} = F_{fastout\_NO3} + F_{slowout\_NO3} + F_{upstream\_NO3} + F_{sewage\_NO3} - F_{downstream\_NO3} + (1 - f_{NIT}) \times R_{stream\_NIT} - R_{stream\_DENIT} \quad (6)$$

where S (g N) represents the N stock in the different reservoirs; F (g N d^{-1}) represents N flow rates between reservoirs following the LSM_Nlateral_off algorithm (Ma et al., 2025) ; R (g N d^{-1}) represents N transformation rates; S_{fast_N}, S_{slow_N}, and S_{stream_N} (g N) represent N (i.e., NH_4^+ or NO_3^-) stocks in the fast, slow, and stream reservoirs, respectively; F_{RO_N} and F_{DR_N} represent N leaching rates via runoff and drainage as simulated by ORCHIDEE3; $F_{fastout\_N}$ and $F_{slowout\_N}$ represent N flow rates from the fast reservoir and slow reservoir to the stream reservoir, respectively; $F_{upstream\_N}$ represents N inflow rates from upstream grids; $F_{downstream\_N}$ represents N outflow rates to downstream grid; F_{sewage_N} represents N inflow rates from sewage; and R_{DON}, R_{NIT}, and R_{DENIT} (g N d^{-1}) represent DON decomposition (Ma et al., 2025), nitrification, and denitrification rates (Ma et al., 2025) in each reservoir r (fast, slow and stream), respectively.

Aquatic nitrification is mechanistically controlled by both NH_4^+ availability and oxygen supply; however, field experiments have generally not identified oxygen limitation as a dominant control on nitrification in river systems (Bernhardt, 2002; Kemp & Dodds, 2002). Consequently, nitrification in rivers is typically more strongly regulated by NH_4^+ availability than by oxygen limitation (Koenig et al., 2017; Pauer & Auer, 2009). At regional to global scales, most river reaches are therefore assumed to remain predominantly oxic, with oxygen availability closely coupled to hydrological transport and organic matter dynamics that are implicitly represented in river network models (Seitzinger et al., 2006; Wollheim et al., 2008). Explicit representation of O_2 dynamics would require spatially continuous, high-resolution dissolved oxygen data that are not available at the global scale and would likely introduce additional uncertainty without commensurate improvements in predictive skill. In addition, nitrification rates in rivers are also strongly controlled by temperature (Shammas, 1986; Zheng et al., 2017; Zhu et al., 2023). Therefore, in ORCHIDEE3-N_{lat}, the nitrification rate in each reservoir r (fast, slow and stream) is simulated using first-order kinetics with respect to NH_4^+ and a temperature dependence, following previous research (Kannel et al., 2007; Pelletier & Chapra, 2006):

$$R_{r\_NIT} = S_{r\_NH4} \times k_{r\_NIT} \times F_{T\_NIT} \quad (7)$$

$$F_{T\_NIT} = e^{-\frac{(TW - T_{ref\_NIT})^2}{(T_{ref\_NIT})^2}} \quad (8)$$

where R_{r_NIT} (g N d^{-1}) represents the nitrification rate in the fast (R_{fast_NIT}), slow (R_{slow_NIT}) or stream (R_{stream_NIT}) reservoirs; S_{r_NH4} represents the NH_4^+ stocks in the fast (S_{fast_NH4}), slow (S_{slow_NH4}) or stream (S_{stream_NH4}) reservoirs; k_{r_NIT} (0.4 d^{-1}) represents the nitrification rate in water at 20°C in the fast, slow and stream reservoirs (Delaware River Basin Commission, 2022; McCutcheon, 1987; Raimonet et al., 2017); F_{T_NIT} (unitless) represents the dependence of nitrification on temperature (Ma et al., 2022); T_{ref_NIT} (= 20°C) is the reference temperature (Zheng et al., 2017), while *TW* is the water temperature, derived from soil temperature using an empirical formulation (Ma et al., 2025; Zhang et al., 2022). DON decomposition rates, as well as flow rates of water, DON and DIN (NH_4^+ and NO_3^-) follow the implementation of LSM_Nlateral_Off (see Ma et al., 2025 for further details). The denitrification rate is represented using a formulation analogous to that of Ma et al. (2025), with the key distinction that the rate is expressed as a function of the NO_3^- stock rather than the total DIN stock.

Following previously published approaches, ORCHIDEE3-N_{lat} represents N_2O emissions from rivers using a constant emission-factor scheme applied to nitrification and denitrification rates:

$$E_{N2O} = f_{NIT} \times R_{NIT} + f_{DENIT} \times R_{DENIT} \quad (9)$$

where E_{N2O} (gN d^{-1}) represents N_2O emissions from rivers to the atmosphere; f_{NIT} (0.9%) and f_{DENIT} (0.9%) represent the emission factors of the nitrification and denitrification pathways (Beaulieu et al., 2011; Maavara et al., 2019; Yao et al., 2020). Note that these emission factors are applied to N transformation processes rather than to N inputs from catchments as in earlier studies (Hu et al., 2016; Kroeze et al., 2005), a key development for accurately representing the kinetics of N_2O production in aquatic systems (Maavara et al., 2019).

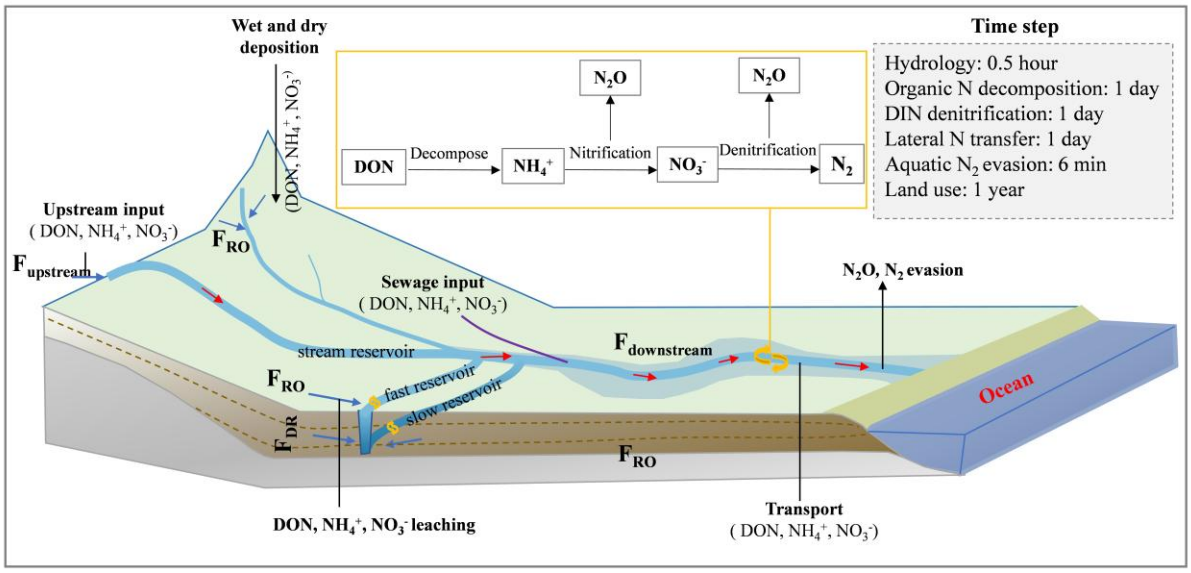

Figure 1. Simulated lateral transfer processes of water and N (DON, NH_4^+ and NO_3^-) and riverine N_2O emissions in ORCHIDEE3-N_{lat}. F_{RO} and F_{DR} are the surface runoff and belowground drainage, respectively. $F_{upstream}$ and $F_{downstream}$ are the upstream inputs and downstream outputs, respectively. Adapted from Fig. 2 in Zhang et al. (2022).

2.2. Data sources

2.2.1. Model forcing data

A historical simulation of ORCHIDEE3-N_{lat} was performed at a spatial resolution of 0.5°, using a set of forcing datasets representing the temporal evolution of meteorological and anthropogenic (land-use and land-management) drivers of the land-river N cycle, as well as databases related to soil properties, and water and N lateral transfers.

Meteorological forcing data (Table 1), including near-surface air temperature, specific humidity, incoming shortwave and longwave radiation, precipitation, snowfall, wind speed, and surface pressure at a 6-hourly time step, were derived from the Climatic Research Unit (CRU) and Japanese Reanalysis (JRA) (CRU-JRA 2.1; Harris et al., 2014). The global annual mean atmospheric CO_2 concentration was obtained from the TRENDY project (Le Quéré et al., 2018). Land-cover distributions were derived by merging LUH2 v2 (Hurtt et al., 2020) with ESA CCI land cover (2022), following Lurton et al. (2020). Soil texture and type followed Reynolds (1999), while soil bulk density and pH were obtained from HWSD v1.2 (FAO/IIASA/ISRIC/ISSCAS/JRC, 2012).

Atmospheric N deposition (NH_x and NO_y) was derived from the IGAC/SPARC Chemistry-Climate Model Initiative (CCMI; Eyring et al., 2013), at a spatial resolution of 0.5° and a monthly temporal resolution. In our simulations, monthly deposition totals were

temporally downscaled to daily values by assuming a uniform deposition rate within each month.

Mineral fertilizer inputs and manure N application to cropland and pasture were obtained from HaNi (Tian et al., 2022). These inputs are provided at an annual temporal resolution and were evenly distributed across each day of the plant growing season (approximately half of the year) in the model simulations. Sewage N inputs (Beusen et al., 2016), available at a 0.5° global resolution with a 5-year time step, was linearly interpolated to an annual time step and subsequently evenly distributed across each day of the year (Table 1). N from sewage was partitioned into different N species following the approach used in Naden et al. (2016), assumimg 10% DON, and 31.5% NH_4^+, 58.5% NO_3^-.

The routing file obtained from Guimberteau et al. (2012) defines the directions of water and N flows directions in each grid cell. The grid-cell-specific topographic index, used to modify water residence time in each reservoir, was derived from Vörösmarty et al. (2000).

Note that, all datasets mentioned above were resampled from native spatial resolutions (see Table 1) to 0.5° for driving ORCHIDEE3-N_{lat}.

2.2.2. Observational data

Water discharge and riverine total N (TN) fluxes simulated by LSM_Nlateral_off have been thoroughly evaluated by Ma et al. (2025). However, compared with LSM_Nlateral_off, ORCHIDEE3-N_{lat} represents N_2O emissions and distinguishes NH_4^+ and NO_3^- by incorporating nitrification into the reaction network, and separating the DIN pool into NH_4^+ and NO_3^- pools.

We thus perform a complementary model evaluation using observed river discharge data from the Global Runoff Data Ccentre (GRDC) (Federal Institute of Hydrology, 2018) and riverine NH_4^+, NO_3^-, DIN and DON concentrations from the Global River water Quality Archive (GRQA) (Virro et al., 2021) to evaluate the model performance in reproducing N lateral transfer processes (Fig. 2). GRDC discharge data were extracted for 346 gauging stations with catchment areas larger than 50,000 km^2. Stations were required to include at least one continuous 12-month period with a minimum 25 observations in per month (Ma et al., 2025). Regarding NH_4^+, NO_3^-, DIN and DON concentrations derived from GRQA, only time series with more than two observations per month in a given year were retained. Where multiple GRQA sites fell within the same 0.5° × 0.5° grid and month, values were averaged to obtain a grid-specific monthly concentration. Applying these criteria, we obtained observed NH_4^+, NO_3^-, DIN and DON data for 98, 103, 28, and 25 grids, respectively. Annual mean concentrations

and fluxes were computed as the arithmetic average of all qualifying observations within each calendar year for each grid:

$$C_{Obs\_N} = \frac{\sum_{im=1}^{12} C_{Obs\_N\_im}}{12} \quad (10)$$

$$F_{Obs\_N} = \sum_{im=1}^{12} C_{Obs\_N\_im} \times F_{Obs\_W\_im} \quad (11)$$

where C_{Obs_N} (g N m^{-3}) and F_{Obs_N} (g N yr^{-1}) represent the annual mean concentrations and fluxes of N (NH_4^+, NO_3^-, DIN or DON here), respectively; $C_{Obs\_N\_im}$ is the observed N concentration (g N m^{-3}) from GRQA for month *im*, and $F_{Obs\_W\_im}$ is the corresponding monthly water discharge (m^3 $month^{-1}$) from the gauging station nearest to the GRQA site.

We additionally compiled riverine N_2O emission observations from 98 sites reported in the peer-reviewed literature (Table S1) and applied the same screening and aggregation procedures as described above, yielding data for 57 grids. Data sources are listed in Table S1.

Table 1. Forcing data used to drive ORCHIDEE3-N_{lat} and datasets used for model evaluation. S_{res} and T_{res} are the spatial and temporal resolution of the forcing data, respectively.

Forcing data	S_{res}	T_{res}	Data source
Meteorological data	0.5°	6 hours	Climatic Research Unit (CRU) and Japanese reanalysis (JRA) data set (CRU-JRA V2.4) (Harris et al., 2014)
CO_2 concentration	/	1 year	TRENDY (Le Quéré et al., 2018)
Land cover	0.5°	1 year	ESA-CCI LUH2v2 (Lurton et al., 2020)
Soil texture class	0.5°	/	(Reynolds et al., 1999)
Soil bulk density and pH	30"	/	HWSD v1.2 (FAO/IIASA/ISRIC/ISSCAS/JRC, 2012)
Fertiliser application	5′	1 year	HaNi (Tian et al., 2022)
Manure application	5′	1 year	HaNi (Tian et al., 2022)
N deposition	0.5	1 year	IGAC/SPARC CCMI
Sewage	0.5	5 years	(Beusen et al., 2016)
Flow direction, Topographic index (f_{topo})	0.5°	/	(Vörösmarty et al., 2000)
Evaluation data	**S_{res}**	**T_{res}**	**Data source**

Riverine water discharge	/	1 day	GRDC[a]
Riverine NH_4^+, NO_3^-, DIN and DON concentration	/	point measurement	GRQA[b]
N_2O emission	/	point measurement	Table S1

[a] Global Runoff Data Centre (GRDC) (Federal Institute of Hydrology, 2018); [b] Global River water Quality Archive (GRQA) (Virro et al., 2021).

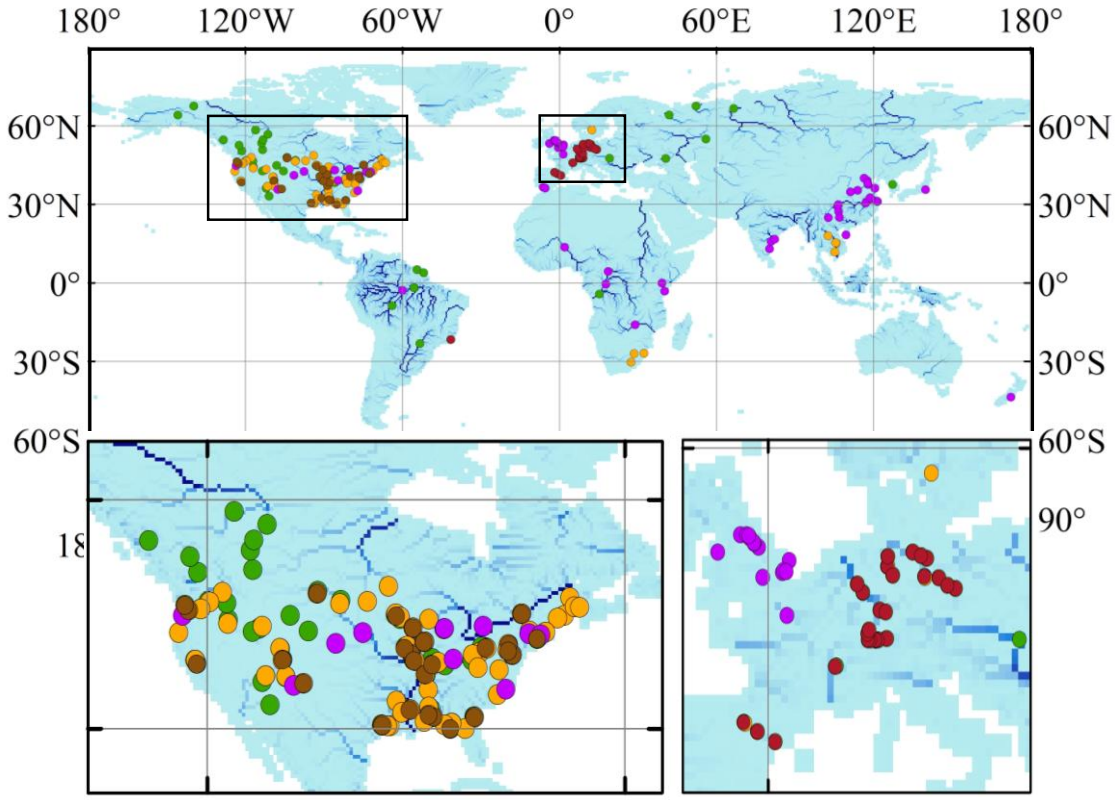

Figure 2. Locations of observational sites for riverine N concentrations and N_2O emission rates. Yellow dots represent sites with NH_4^+ concentration data, 98 sites; green dots represent sites with NO_3^-concentration data, 103 sites; red dots represent sites with DIN concentration data, 28 sites; brown dots represent sites with DON concentration data, 25 sites; purple dots represent sites with riverine N_2O emission data, 57 sites. Insets for data-dense regions in North America and Europe are also shown.

3. Results and discussion

3.1. Model evaluation

Previous results showed that for major rivers with drainage areas exceeding 50, 000 km^2 worldwide, ORCHIDEE reliably reproduces the magnitude and seasonal variations of

lateral water and TN fluxes (Ma et al., 2025; Zhang et al., 2022). To further assess ORCHIDEE3-N_{lat}, we evaluate its performance in simulating riverine concentrations and fluxes of NH_4^+, NO_3^-, DIN, and DON, as well as riverine N_2O emissions. As shown in Fig. 3, using logarithmic-transformed values, the model explains 53%, 70%, 65% and 78% of the spatial variations in observed long-term mean NH_4^+, NO_3^-, DIN, and DON concentrations, respectively, and 60 % of the spatial variations in N_2O emissions. When evaluated on a linear scale, the corresponding values are 51%, 68%, 65%, and 78%, indicating comparable model performance across scales. For N fluxes, based on logarithmic-scale comparisons, the model explains 62%, 44%, 45% and 55% of the spatial variations in observed NH_4^+, NO_3^-, DIN, and DON, respectively. When evaluated on a linear scale, the corresponding values increase to 79%, 63%, 70% and 88% (Fig. S1). Notably, although NH_4^+ exhibits the weakest correlation for the concentrations, it exhibits the strongest correlation for the fluxes (R^2 = 0.62). ORCHIDEE3-N_{lat} does not directly simulate N concentrations, instead, daily N concentrations are calculated by dividing N stock by water volume in the stream reservoir. Consequently, bias in discharge or water storage at a given site may propagate into concentration errors. Overall, the joint evaluation of concentrations and fluxes indicates that the model is robust in simulating lateral N transport and transformation, as well as riverine N_2O emissions at the global scale.

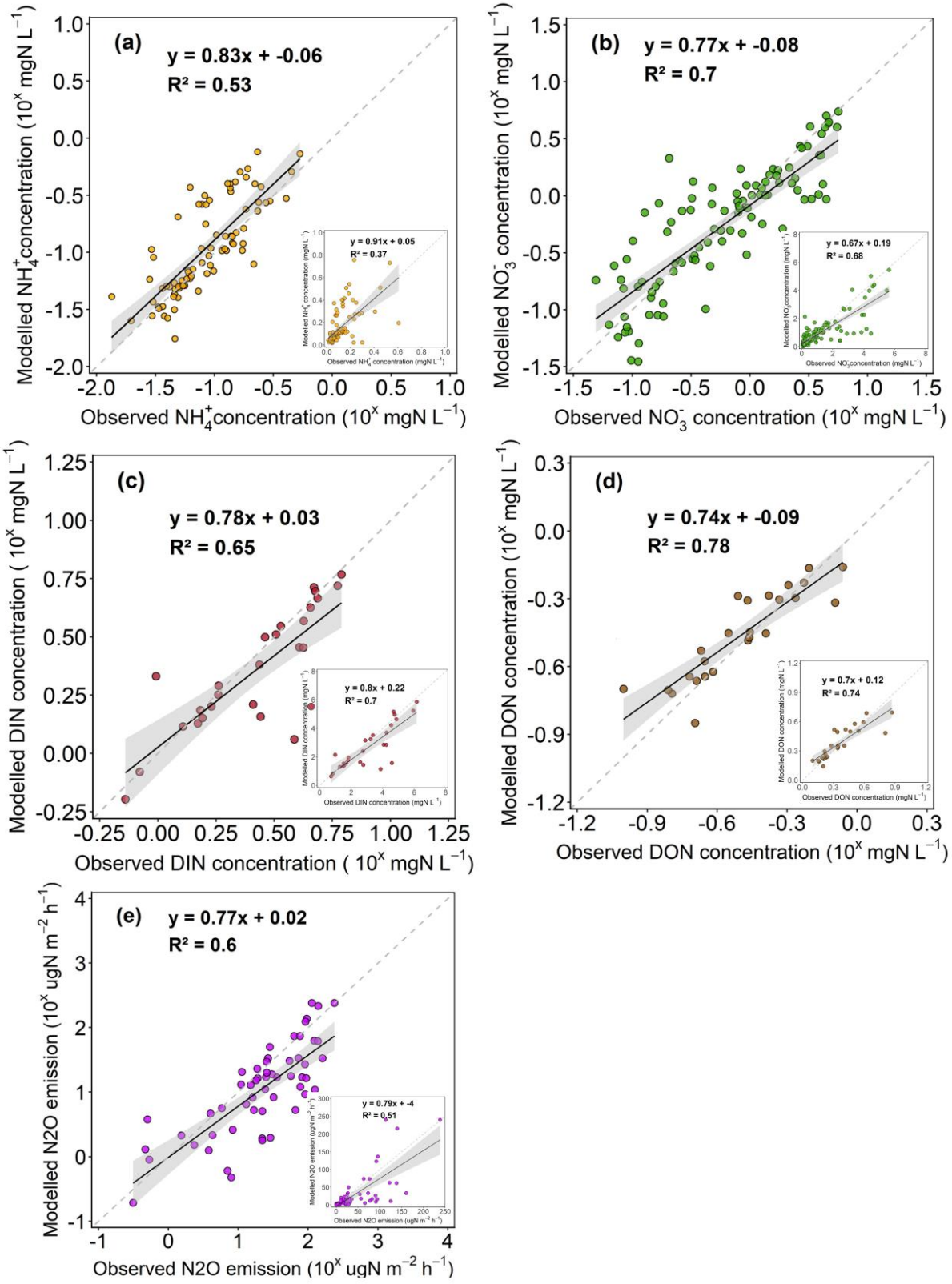

Figure 3. Comparison of observed and modeled annual mean concentrations of NH_4^+ (a), NO_3^- (b), DIN (c), and DON (d), as well as riverine N_2O emission rates (f). The larger panels use a logarithmic scale; the insets show the same data on a linear scale. "Con" represents concentration, "Em" represents emission.

3.2. Historical trajectories of global riverine N fluxes and N_2O emissions

Global application of our model indicates that riverine N fluxes have increased substantially from 1901 to 2020, with species-specific trajectories (Fig. 4). Averaged over 2001–2020, averaged DIN inflow into rivers and export to the ocean were 39.9 and 23.8 Tg N yr^{-1}, representing dramatic increases of 245% and 151% relative to 1901–1920. Over the same periods, annual DON inflow into rivers and export to the ocean were 18.9 and 10.8 Tg N yr^{-1}, increasing by 38% and 32%, respectively. Piecewise analysis indicates a pronounced acceleration in DIN fluxes after 1965, with growth rates rising from 0.05 to 0.25 Tg N yr^{-2} (i.e., 0.25 Tg N yr^{-1} per year) for terrestrial DIN inputs to rivers and from 0.07 to 0.54 Tg N yr^{-2} for riverine export to the ocean. In contrast, DON fluxes increased more rapidly prior to 1965. These divergent trajectories lead to an increasing DIN:DON ratio in river flows, consistent with observation syntheses showing a shift from heterogeneous mixtures of N species toward inorganic dominance under intensifying human disturbances (Wymore et al., 2021). Trends simulated by ORCHIDEE3-N_{lat} closely match those from offline model (LSM_Nlateral_off, Ma et al., 2025), with minor differences attributable to climate forcing datasets and process representations in the two models.

Riverine N_2O emissions likewise increased sharply by about 226%, from 111.7 Gg N yr^{-1} (1901–1920) to 365.0 Gg N yr^{-1} (2001–2020). The trajectory was non-monotonic, with mean growth rates of 0.78 Gg N yr^{-2} during 1901–1965 and 4.80 Gg N yr^{-2} after 1965. DLEM simulations show similar behaviour until the mid-1990s, followed by a decline over 1996–2016 (-1.03 Gg N yr^{-2}). To investigate the mechanisms responsible for the differences in riverine N_2O emissions between DLEM and ORCHIDEE3-N_{lat} during the last two decades, we compared key forcing datasets used by the two models, including air temperature, precipitation, N fertilizer, N manure application, and atmospheric N deposition (Fig. S2). These datasets exhibit no obvious differences between the two models over 1995–2016. Direct comparison of sewage inputs is not possible due to data limitations. However, Yao et al. (2020) reported that sewage accounts for about 2.9% of terrestrial N inflow to rivers, whereas ORCHIDEE3-N_{lat} simulated a larger and increasing contribution (5%–16%). This discrepancy suggests that differences in sewage inputs may partly explain divergences in simulated riverine N_2O emissions. In addition, differences in model structure and parameterization likely contribute to these discrepancies, underscoring the importance of model intercomparisons, such as the global N_2O Model Intercomparison Project (NMIP) for reducing uncertainties and improving confidence in riverine N_2O simulations.

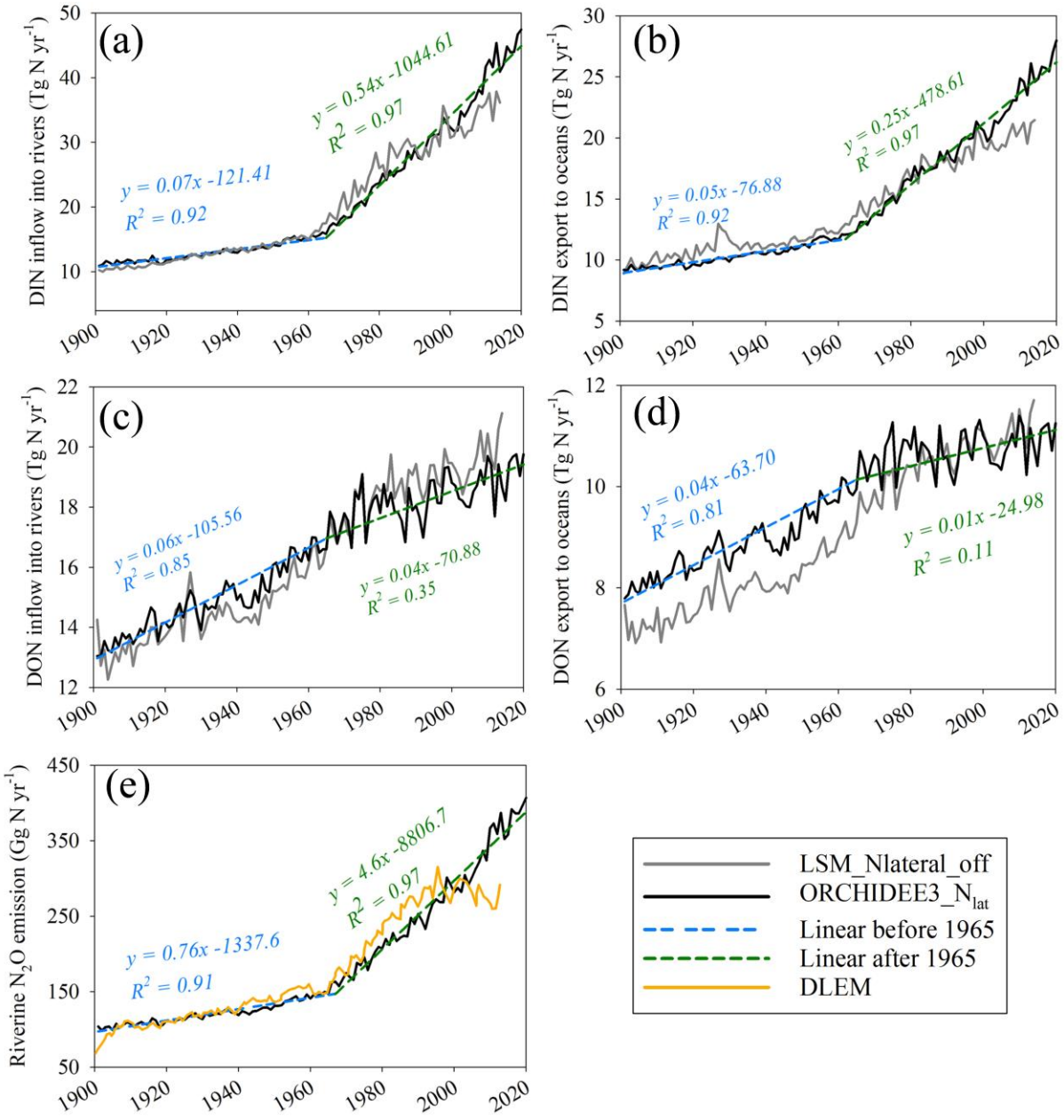

Figure 4. Trends in global N fluxes and N_2O emissions over 1901–2020 simulated by ORCHIDEE3-N_{lat}, LSM_Nlateral_off, and DLEM: (a) DIN inflow into rivers; (b) DIN export to the ocean; (c) DON inflow into rivers; (d) DON export to the ocean; (e) riverine N_2O emissions.

3.3. Spatial patterns of global riverine N_2O emission

Riverine N_2O emissions exhibit pronounced spatial heterogeneity in both the early 20th century (1901–1920 mean) and the contemporary period (2001-2020 mean), with elevated values concentrated in in tropical regions and intensively cultivated croplands, including eastern North America, South America (excluding arid areas), Western Europe, tropical Africa, South Asia, Southeast Asia, and southeastern China (Fig. 5a–b). A similar spatial pattern is

found for N_2O emission densities (i.e., N_2O emissions per river area), identifying these regions as persistent hotspots. Consistent with this, an observation-based machine-learning (ML) assessment by Marzadri et al. (2021) reports high N_2O emission densities in the same regions, providing independent support for the spatial patterns simulated by ORCHIDEE3-N_{lat}.

However, N_2O emission densities simulated by ORCHIDEE3-N_{lat} differ from those reported by Marzadri et al. (2021) in several regions, including Argentina, parts of southern Africa (e.g., Namibia, Botswana, and the country South Africa), and parts of Russia (Fig. S4). These discrepancies likely arise from two main factors. First, the two products differ substantially in spatial resolution, ORCHIDEE3-N_{lat} simulations are produced at a resolution of 0.5°, whereas the Marzadri product is resolved at 30 arc-seconds. The finer resolution allows for a more explicit representation of localized N_2O emission hotspots, which may be smoothed or masked at coarser scales. Second, the ML-based DIN product used to drive the N_2O model in Marzadri et al. (2021) was trained primarily on North American observations (Shen et al., 2020). Its global application therefore introduces additional uncertainty, particularly in regions with hydroclimatic and biogeochemical conditions that are underrepresented in the training data (Liu et al., 2023). Hydrological and biogeochemical processes in Argentina, Russia, and southern Africa (including Namibia, Botswana, and the country South Africa) differ fundamentally from those in the North America (Dargie et al., 2017; McClelland et al., 2012; Regnier et al., 2013).

Compared with the early 20th century, present-day riverine N_2O emissions have increased across most regions, with the largest increases (> 500%) in the western United States, the eastern coastal area of South America, the northern Mediterranean littoral, South and Southeast Asia, and southeastern China (Fig. 5c), whereas slight decreases are evident in the Amazon basin and parts of tropical Africa. Measurements from hotspot regions indicate that elevated riverine N_2O emissions are primarily driven by anthropogenic inputs, including fertilizer application, wastewater discharge, and eutrophication (Beaulieu et al., 2011; Laini et al., 2011; Li et al., 2022; Upadhyay et al., 2026). These N enrichments, often amplified by hydrological regulation and low-oxygen conditions, provide a mechanistic explanation for the simulated increases in these regions. In contrast, declining riverine N_2O emissions in parts of the Amazon Basin and tropical Africa are associated with limited anthropogenic N inputs and rising atmospheric CO_2. Previous studies show that N inputs in these regions have remained relatively low (Lamarque et al., 2013; Lu & Tian, 2017; Tian et al., 2022). In addition, in these generally N-limited rainforest ecosystems (LeBauer & Treseder, 2008; Wright et al., 2018),

elevated CO_2 enhances plant C sequestration and N uptake (Ainsworth & Long, 2021; Drake et al., 2013), thereby slightly reducing N leaching (Ma et al., 2025) and associated riverine N_2O emissions.

The latitudinal pattern of riverine N_2O emissions indicates that, during the historical period, subtropical regions have replaced the tropics and high latitudes as the zones of highest emission intensity (Fig. 5d). By contrast, DLEM outputs show a peak in temperate latitudes (Yao et al., 2020). This difference largely stems from our substantially higher subtropical emissions, particularly across South Asia, where intensive human activities and large N inputs (including N inputs from urban sewage, S3) drive exceptionally high N inflows into rivers (Ma et al., 2025; Tian et al., 2022), and consequently elevated N_2O emissions. Moreover, the observation-based ML assessment (Marzadri et al., 2021) reports high N_2O emission densities in South Asia, providing further support for our simulations and for a peak in emissions in the northern subtropics (Fig. S4).

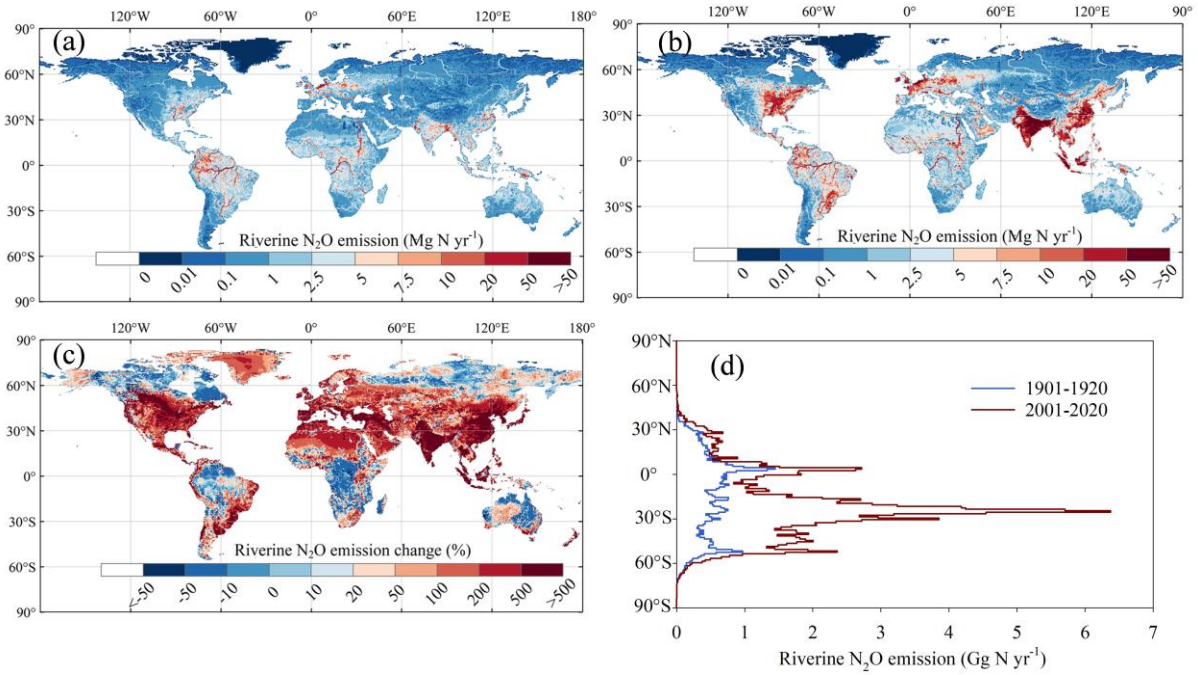

Figure 5. Spatial patterns of annual mean riverine N_2O emissions: (a) 1901–1920; (b) 2001–2020; (c) changes in emissions from 1901–1920 to 2001–2020; (d) latitudinal distribution of N_2O emissions in the early 20th century and the contemporary period.

3.4. Drivers of the historical increase in global riverine N fluxes and N_2O emissions

Since the early 20th century, anthropogenic drivers have substantially increased lateral N fluxes and riverine N_2O emissions. We implemented a series of factorial experiments to attribute these changes to the respective drivers (Table. S2). As shown in Fig. 6a–b, during

1901–1969, atmospheric N deposition and sewage were the primary factors of increased DIN inflows to rivers and exports to the ocean. Manure application contributes more to DIN exports than to inflows, as a substantial fraction of manure-derived organic N is transformed into DIN during lateral transfer. From the 1970s onward, widespread land-use change and rising fertilizer use (Tian et al., 2022) became the main drivers of enhanced DIN lateral transfer to rivers and export to the ocean. In the 2010s, fertilization contributed 19.5 Tg N yr^{-1} to DIN inflow and 8.6 Tg N yr^{-1} to ocean export, comparable to the combined contributions of N deposition and sewage. Conversely, CO_2 fertilization has reduced DIN transfer since the 1970s by enhancing plant N uptake and biomass sequestration (Johnson et al., 2004; Niklaus et al., 2001; Terrer et al., 2019), and hence to a decrease in DIN lateral transfer. By the 2010s, its contribution reached -7.6 Tg N yr^{-1} for DIN inflow and -3.8 Tg N yr^{-1} for DIN export.

Regarding DON, lateral transfer increased over 1901–2020, with manure application explaining over 75% of the increase (Fig. 6 c–d). This prominent role of manure is consistent with evidence that manure substantially enhances soil organic N accumulation, enlarging the pool susceptible to lateral mobilization (Denoncourt et al., 2025). Event-scale and field studies further show that storm-driven transport efficiently mobilizes manure-derived DON and that manure application alters dissolved organic matter composition and mobility, increasing potential DON export during hydrologically active periods (Begum et al., 2022; Luek et al., 2020). In contrast, atmospheric NH_4^+ and NO_3^- deposition, and mineral fertilizer application contribute negatively DON lateral transfer trends. In the 2010s, the fertilizer contribution to DON inflow and export were -1.2 Tg N yr^{-1} and -0.6 Tg N yr^{-1}, respectively. In ORCHIDEE3-N_{lat}, inorganic N inputs alleviate N limitation, enhancing vegetation growth and evapo-transpiration, thereby reducing runoff, drainage, and DON leaching. However, field evidence remains mixed: some studies report reduced DON fluxes due to increased evapotranspiration (Farley et al., 2005), whereas others show enhanced DON leaching under long-term N addition (Feng et al., 2023; McDowell et al., 2004). Global-scale assessments of this process remain lacking. Elevated CO_2 exerts a positive effect on DON transfer (Fig. 6c). In ORCHIDEE3-N_{lat}, CO_2 fertilization increases organic matter inputs (via productivity, litterfall, and root exudation) and reduces stomatal conductance, thereby enhancing runoff and drainage. Together, increased DON supply and water fluxes promote DON lateral transfer fluxes. A 5-year field experiment at the alpine treeline reported that CO_2 enrichment stimulated microbial activity and soil respiration, and increased soil DOC and DON concentrations, thereby enhancing the potential for DOC and DON leaching (Hagedorn et al., 2008). While large-scale reconstructions such as those by Nakhavali et al. (2024) focus on DOC rather than DON, they provide complementary

evidence for enhanced DOM mobilization under rising CO_2, which is consistent with the process-level mechanisms driving DON leaching in ORCHIDEE3-N_{lat}.

Attribution results for riverine N_2O emissions broadly follow those for DIN. During 1901–1969, atmospheric N deposition, manure application and sewage N were the primary drivers of the increasing emissions. Over the 1970–2020 period, climate change, land-use change and especially fertilizer use exerted progressively stronger influences. By the 2010s, fertilization contributed 166.1 Gg N yr^{-1} to riverine N_2O emissions, approximately equal to the combined contributions of all other factors. Elevated atmospheric CO_2 reduced the intensity of DIN lateral transfer, and thus riverine N_2O emissions, with a contribution of -27.7 Gg N yr^{-1} in the 2010s, partly offsetting increases driven by climate change and land-use change. These attribution results are broadly consistent with DLEM (Yao et al., 2020), with both models showing a negative effect of CO_2. DLEM excluded land-use change and sewage inputs as potential drivers in their attribution analysis. While previous studies suggest that sewage contributes only ~2.9% of terrestrial N inputs to rivers (Beaulieu et al., 2011; Yao et al., 2020), our results indicate a larger and increasing contribution (5.4–14.6%; Ma et al., 2025). Correspondingly, sewage-driven N_2O emissions rose from 12.0 Gg N yr^{-1} in the 1900s to 77.2 Gg N yr^{-1} in the 2010s. Our findings highlight the importance of accounting for urban sources, particularly wastewater discharge in future attribution analyses of riverine N_2O emissions.

Overall, anthropogenic N inputs are the dominant driver of lateral N fluxes and riverine N_2O emissions worldwide, although their relative importance varies markedly among continents (Fig. 7 & S5). Asia exhibits the most pronounced increase in riverine N_2O emissions (Fig. 7c), with fertilizer and manure application becoming dominant drivers after the 1960s, reflecting rapid intensification of agricultural activities. North America (Fig. 7a) also showes substantial increases, driven primarily by fertilizer in the contemporary period. Europe is the only continent that exhibiting decreasing riverine N_2O emissions after the 1980s, with N inputs (fertilizer, manure application and sewage) remaining the dominant contributors. In South America, increases arise from relatively balanced contributions of fertilizer use, manure application, sewage and land-use change. In Africa and Oceania, atmospheric N deposition dominates trends of riverine N_2O emissions (Fig. 7e & 7f). Drivers of lateral N fluxes also vary across continents (Fig. S5). Patterns of DIN export to the ocean broadly mirror those of riverine N_2O emissions. For DON export to the ocean, manure application explains most of the temporal evolution in Asia, North America, and Europe (Fig. S5), whereas in Africa, South America, and Oceania, manure and land-use change are the primary drivers (Fig. S5).

Fig. S6 reveals clear temporal and regional differences in the drivers of changing lateral N fluxes. During the early 20th century (1901–1920), agricultural activities (including mineral fertilizer use, manure application, and land-use change) exerted noticeable influences on DON inflow into rivers in many regions (Fig. S6 a1), whereas anthropogenic contributions to DIN inflow and riverine N_2O emissions were comparatively weak (Fig. S6 b1 & c1). By the early 21st century (2001–2020), agriculture became the dominant drivers of DIN and DON inflows into rivers, as well as riverine N_2O emissions, especially in Europe, North America, and East and South Asia (Fig. S6 a2–c2). Sewage inputs also exerted notable influences in densely populated regions (Fig. S6 a2–c2). Similar spatial patterns are observed for DIN and DON export to the ocean (Fig. S6 d2–e2), with agricultural sources increasingly dominating N export across many river basins.

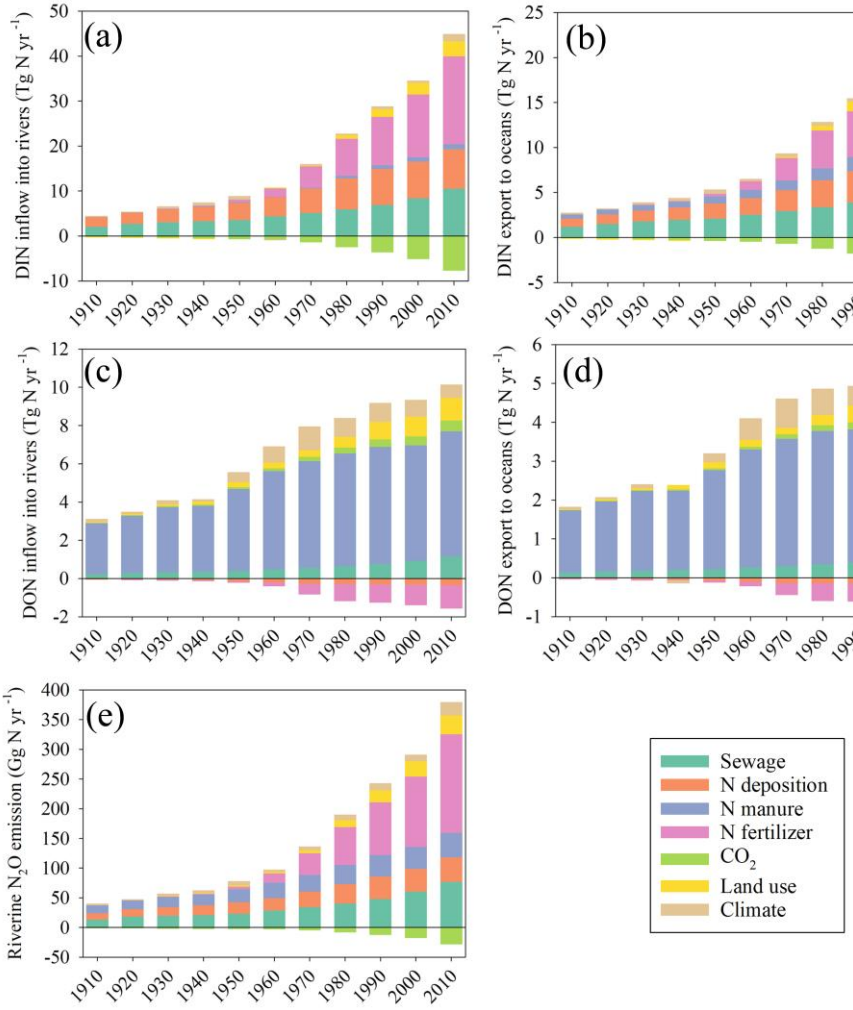

Figure 6. Attribution analysis of N fluxes and riverine N_2O emissions over 1901–2020: (a) DIN inflow into rivers; (b) DIN export to the ocean; (c) DON inflow into rivers; (d) DON export to the ocean; (e) riverine N_2O emissions. Note that the scales differ among N fluxes.

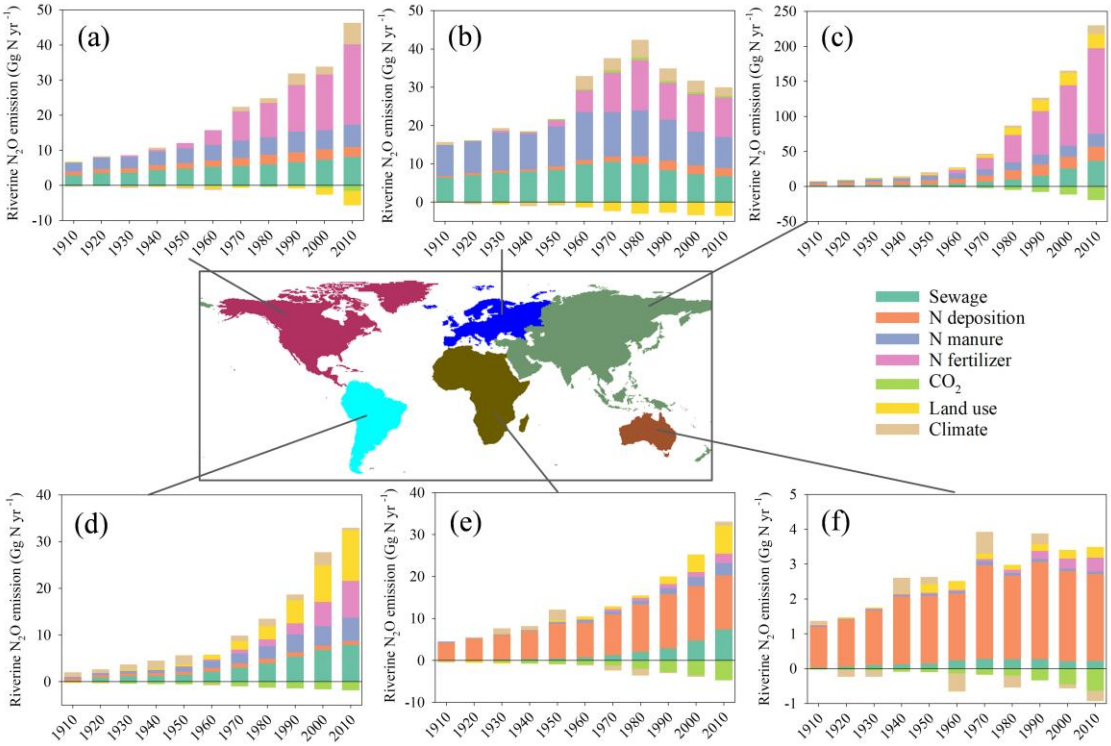

Figure 7. Attribution analysis of riverine N_2O emissions over 1901–2020 across continents: (a) North America; (b) Europe; (c) Asia; (d) South America; (e) Africa; (f) Oceania. See Fig. S5 for the corresponding continental-scale analysis of lateral N fluxes.

3.5. Global Land-river N cycling and budget

Based on ORCHIDEE3-N_{lat} simulations for 1900–1920 and 2000–2020, we constructed a new global land-river N budget using the scheme proposed by Gruber & Galloway (2008, Fig 8). In the early 20th century (blue arrows), terrestrial Nr was close to steady state, with inputs of 97 Tg N yr^{-1} and output of 95 Tg N yr^{-1}, including 69 Tg N yr^{-1} emitted to the atmosphere and 25 Tg N yr^{-1} were exported laterally to rivers (Fig. 8). In the early 21st century, anthropogenic perturbations more than doubled terrestrial Nr inputs to 254 Tg N yr^{-1}, with fertilizer accounting for ~80% of the increase. Gaseous N emissions from land to atmosphere did not rise proportionally: N_2 outgassing increased by 53%, NO_x by 33%, N_2O by 25%, and NH_3 by 38%. The relatively modest increase in N_2O suggests a declining emission factor under higher N loading, consistent with nonlinear responses observed in some field studies (Gu et al., 2019; Wu et al., 2023), although contrasting evidence exists (Shcherbak et al., 2014; Takeda et al., 2024). In contrast, dissolved N (DON and DIN) inputs to rivers more than doubled, from 25 Tg N yr^{-1} in the early twentieth century to 59 Tg N yr^{-1} in the contemporary period (Fig. 8). PON lateral transfer is not included in the current ORCHIDEE3-N_{lat}, however, our offline simulation (LSM_Nlateral_off) indicates an average annual PON

input of 12 Tg N yr^{-1} with no discernible trend over 1901–2014. On this basis, we estimate that total N delivered to rivers increased from 37 Tg N yr^{-1} in the early 20th century to 71 Tg N yr^{-1} in the contemporary period (Fig. 8). Consistent with this estimate, Vilmin et al. (2018), using IMAGE-GNM, reported an increase in global land-to-river TN from 35 Tg N yr^{-1} in 1900 to 68 Tg N yr^{-1} in 2000. Within the river network, our simulations show that N_2 emissions rose by ~200%, while N_2O emissions rose by about 300% from ~0.10 Tg N yr^{-1} (1901–1920) to ~0.40 Tg N yr^{-1} (2001–2020) (Fig. 8). The decadal mean N_2O emission during 2001–2010 was 0.33 Tg N yr^{-1}. Over 1901-2010, DLEM simulated a riverine N_2O emissions increase from 0.09 to 0.29 Tg N yr^{-1}, while IMAGE-DGNM simulated vales from 0.35 to 0.70 Tg N yr^{-1} (Wang et al., 2023). Our estimates fall within the range delineated by these two models. TN (DIN, DON, PON) export to the ocean increased by 61% over the past century, from 28 to 45 Tg N yr^{-1} (Fig. 8), consistent with previous model simulations, see Ma et al. (2025) for further details. The contemporary estimate (45 Tg N yr^{-1}) falls within the range reported by previous model simulations (35–49 Tg N yr^{-1}) (Boyer et al., 2006; Green et al., 2004; Lee et al., 2024a; Mayorga et al., 2010; Vilmin et al., 2018).

The global N cycle synthesized by Gruber and Galloway (2008) provides a conceptual, observation-constrained framework of the N cycle by integrating major N sources, sinks, and transfers across the atmosphere, terrestrial ecosystems, and the ocean. ORCHIDEE3-N_{lat} now provides results from a fully coupled, internally consistent process-based model that explicitly represents lateral N transfer, in-stream N transformations, and associated N_2O emissions along the land-river water continuum. Under natural conditions in Gruber and Galloway (2008), corresponding to ORCHIDEE3-N_{lat} simulations for 1901–1920, the land-ocean N connectivity is similar. This can be illustrated by the fraction of N exported to the ocean relative to that entering terrestrial ecosystems, which is approximately 23% in Gruber and Galloway (2008) and 27% for ORCHIDEE3-N_{lat}. However, in the contemporary period, ORCHIDEE3-N_{lat} simulates weaker land-ocean N connectivity (~18%), reflecting lower land-ocean connectivity and an intensification of the filtering role of the global river network. By contrast, Gruber and Galloway (2008) report a higher value (~25%) for the anthropogenically influenced period, likely due to their larger assumed riverine N export (~70 Tg N yr^{-1}) compared with more recent estimates. These discrepancies highlight the need for improved observational constraints on riverine N export to the ocean to reduce uncertainties in model simulations, similarly to what has recently been achieved for the C fluxes (Liu et al., 2024).

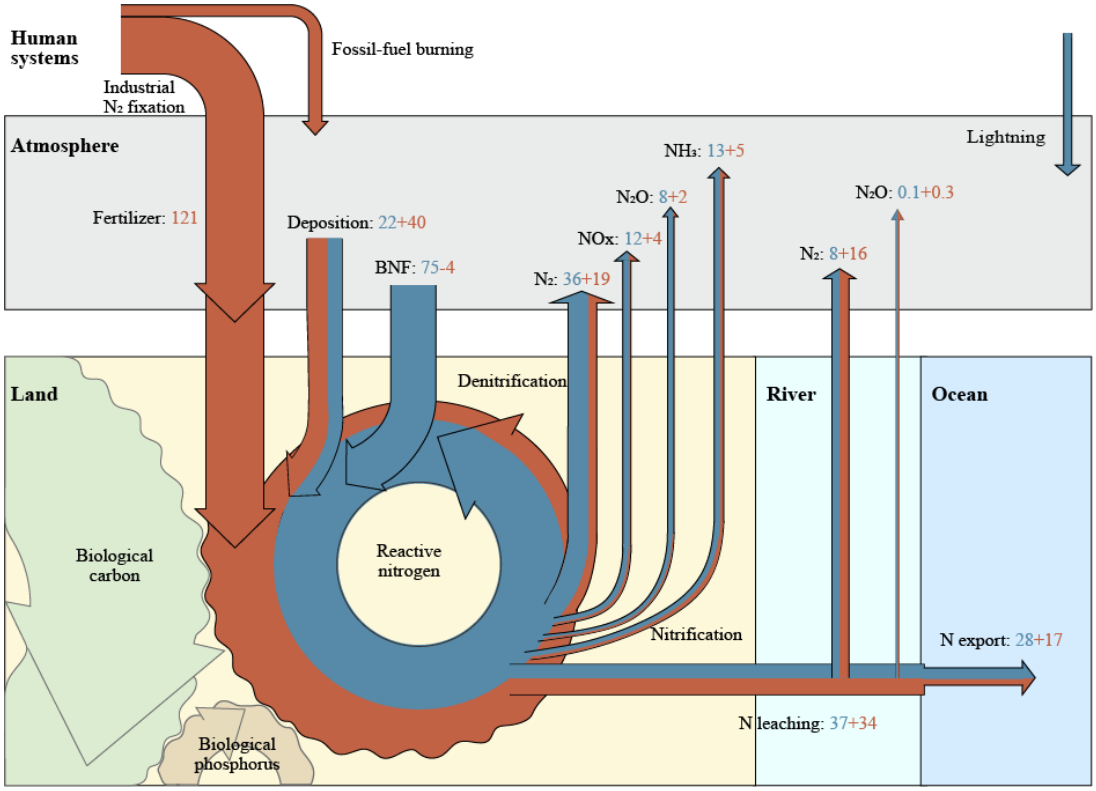

Figure 8. Depiction of the global land-river N cycle. Blue fluxes represent the early 20th century (mean values for 1901–1920), while orange fluxes represent anthropogenic perturbations relative to this baseline. Modified from Gruber and Galloway (2008).

3.6. Model limitations

In ORCHIDEE3-N_{lat}, soil DON leaching is estimated using an empirical formulation based on soil C content and the soil C:N ratios. This is a limitation, as numerous studies have reported a decoupling of soil C and N cycles, particularly under N addition, with DON often responding more rapidly than DOC (Gao et al., 2015; McDowell et al., 2004). Consequently, the model simulates a negative response of DON leaching to inorganic N addition, as fertilization-induced reductions in runoff and drainage outweigh increases in DON concentration. This feedback remains uncertain and calls for additional observations of DON concentrations in soils and rivers, together with targeted manipulation experiments to improve the mechanistic representation of soil DON dynamics and leaching processes in models. PON erosion is omitted, and the model focuses on DIN and DON, which exhibit obvious temporal trends compared to the particulate phase (Ma et al., 2025). In principle, PON erosion could be estimated analogously to POC by applying sediment delivery rates to topsoil organic N (Zhang et al., 2020; 2022); ORCHIDEE3-N_{lat} also currently omits the role of river floodplain dynamics and channel erosion due to limited understanding and lack of robust parameterizations at the

global scale. Floodplains regulate N lateral transfer through exchange, retention, and transformation processes. Site-scale studies show that by expanding the water–soil–vegetation contact and increasing residence time, floodplains promote redox conditions that enhance denitrification and thereby reduce downstream NO_3^- loads (Gordon et al., 2020; Mayer et al., 2007; Roley et al., 2012; Tschikof et al., 2022); they also trap and store particulate N in over-bank deposits and modulate DON dynamics during inundation and drawdown (Noe & Hupp, 2005; Zuijdgeest et al., 2015). However, integrating these processes into global models is strongly constrained by limited observations across diverse hydroclimatic and geomorphic settings, highlighting the need for coordinated, large-scale observational efforts. In addition, N retention and recycling in lakes and artificial reservoirs are not currently represented in the model; these systems provide favourable conditions for N burial in sediments and permanent loss via denitrification (Saunders and Kalff, 2001; Harrison et al., 2009; Akbarzadeh et al., 2019). The absence of these processes may result in an underestimation of N removal in inland waters and N leaching from land, and an overestimation of N exports to oceans.

Model evaluation of ORCHIDEE3-N_{lat} against 57 observation sites indicates that the model reproduces the first-order magnitude and broad spatial patterns of riverine N_2O emissions, providing a practical baseline for global simulations. However, ORCHIDEE3-N_{lat} does not explicitly represent N cycling and N_2O processes in the hyporheic zone. Strong redox gradients and active water–sediment exchange in this zone can enhance coupled nitrification–denitrification and N_2O production (Li et al., 2023; Wang et al., 2024), and their omission may lead to an underestimation of riverine N_2O emissions. Addressing this limitation will be an important focus of future model development. In addition, observational network remains sparse and unevenly distributed. Globally, fewer than 30 stations provide DIN and DON data; DIN observations are concentrated in Western Europe, whereas DON records are primarily from North America. N_2O measurements are likewise limited to 57 sites. This paucity of observations hampers parameter identification in global-scale lateral N transfer models and inflates predictive uncertainty (Wellen et al., 2015), underscoring the need for expanded, spatially representative monitoring of N fluxes and riverine N_2O emissions, particularly DON.

4. Conclusion

In this study, we developed ORCHIDEE3-N_{lat}, a global land-river modelling framework that explicitly represents lateral N transfer, in-stream N transformations, and riverine N_2O emissions, and applied it to reconstruct their historical evolution over 1901–2020 at 0.5° resolution globally. By coupling terrestrial N cycling with riverine transport and in-

stream processes, the model enables a consistent assessment of how anthropogenic perturbations propagate through river networks and affect N export to the ocean and riverine N_2O emissions. Simulations reveal a pronounced century-scale shift toward inorganic N dominance in riverine fluxes. DIN inflow to rivers and exports to the ocean increased strongly, particularly after the 1960s, whereas DON increased more modestly, indicating divergent responses of inorganic and organic N to anthropogenic forcing. Consistent with the enhanced lateral N transfer, riverine N_2O emissions increased by more than 200% over the twentieth century, with contemporary hotspots concentrated in intensively managed subtropical regions. Attribution analyses reveal contrasting controls on dissolved N forms: DIN is dominated by atmospheric deposition, sewage, and fertilizer inputs, whereas DON primarily regulated by manure inputs and hydroclimatic variability. Riverine N_2O emissions broadly track DIN but with an enhanced contribution from manure application. Anthropogenic impacts on N fluxes and riverine N_2O emissions vary across continents, with Europe being the only region showing a decline both in N fluxes and riverine N_2O emissions after the 1980s. Globally, anthropogenic perturbations since 1900 have more than doubled terrestrial N inputs, whereas N export to the ocean increased by only 61%, reflecting reduced land-ocean connectivity, and enhanced N removal within land and river systems. ORCHIDEE3-N_{lat} has several limitations that point to priorities for future development, including the explicit representation of soil DON dynamics and PON erosion, as well as inclusion of N cycling and N_2O emission in other inland water bodies. These advances should be accompanied by expanded observational datasets for model further calibration and evaluation. Ultimately, ORCHIDEE3-N_{lat} provides a foundation for coupling with ocean biogeochemistry models such as PISCES (Bopp et al., 2013; Martinez-Rey et al., 2015) within the IPSL-ESM, enabling integrated simulations of N cycling and N_2O emissions across the land-river-ocean continuum and their feedbacks to climate change and anthropogenic disturbance.

Acknowledgement

This research was supported by the European Union's Horizon 2020 research and innovation program ESM-2025 under grant agreement No. 101003536 and by BELSPO through the project ReCAP (part of the Belgian research programme FedTwin). This work was also supported by the National Key Research and Development Program of China (Grant No. 2025YFE0108800), the Young Scientists Project of National Key R&D Program of China (No. 2024YFF0811000), and the Basic Research Funds for Higher Education Institutions, Sun Yat-sen University (37000-12255010) also supported this study.

Reference

Ainsworth, E. A., & Long, S. P. (2021). 30 years of free-air carbon dioxide enrichment (FACE): What have we learned about future crop productivity and its potential for adaptation? *Global Change Biology*, *27*(1), 27–49. https://doi.org/10.1111/gcb.15375

Akbarzadeh, Z., Maavara, T., Slowinski, S., & Van Cappellen, P. (2019). Effects of damming on river nitrogen fluxes: A global analysis. Global Biogeochemical Cycles, 33, 1339–1357. https://doi.org/10.1029/2019GB006222

Aumont, O., Ethé, C., Tagliabue, A., Bopp, L., & Gehlen, M. (2015). PISCES-v2: An ocean biogeochemical model for carbon and ecosystem studies. *Geoscientific Model Development*, *8*(8), 2465–2513. https://doi.org/10.5194/gmd-8-2465-2015

Baron, J. S., Hall, E. K., Nolan, B. T., Finlay, J. C., Bernhardt, E. S., Harrison, J. A., Chan, F., & Boyer, E. W. (2013). The interactive effects of excess reactive nitrogen and climate change on aquatic ecosystems and water resources of the United States. *Biogeochemistry*, *114*(1), 71–92. https://doi.org/10.1007/s10533-012-9788-y

Battin, T. J., Lauerwald, R., Bernhardt, E. S., Bertuzzo, E., Gener, L. G., Hall, R. O., Hotchkiss, E. R., Maavara, T., Pavelsky, T. M., Ran, L., Raymond, P., Rosentreter, J. A., & Regnier, P. (2023). River ecosystem metabolism and carbon biogeochemistry in a changing world. *Nature*, *613*(7944), 449–459. https://doi.org/10.1038/s41586-022-05500-8

Beaulieu, J. J., Tank, J. L., Hamilton, S. K., Wollheim, W. M., Hall, R. O., Mulholland, P. J., Peterson, B. J., Ashkenas, L. R., Cooper, L. W., Dahm, C. N., Dodds, W. K., Grimm, N. B., Johnson, S. L., McDowell, W. H., Poole, G. C., Valett, H. M., Arango, C. P., Bernot, M. J., Burgin, A. J., Thomas, S. M. (2011). Nitrous oxide emission from denitrification in stream and river networks. *Proceedings of the National Academy of Sciences*, *108*(1), 214–219. https://doi.org/10.1073/pnas.1011464108

Begum, M. S., Lee, M.-H., Park, T. J., Lee, S. Y., Shin, K.-H., Shin, H.-S., Chen, M., & Hur, J. (2022). Source tracking of dissolved organic nitrogen at the molecular level during storm events in an agricultural watershed. *Science of The Total Environment*, *810*, 152183. https://doi.org/10.1016/j.scitotenv.2021.152183

Bernhardt, P. A. (2002). The modulation of sporadic-E layers by Kelvin–Helmholtz billows in the neutral atmosphere. *Journal of Atmospheric and Solar-Terrestrial Physics*, *64*(12), 1487–1504. https://doi.org/10.1016/S1364-6826(02)00086-X

Beusen, A. H. W., Bouwman, A. F., Van Beek, L. P. H., Mogollón, J. M., & Middelburg, J. J. (2016). Global riverine N and P transport to ocean increased during \hack\newlinethe 20th century despite increased retention \hack\newlinealong the aquatic continuum. *Biogeosciences*, *13*(8), 2441–2451. https://doi.org/10.5194/bg-13-2441-2016

Billen, G., Garnier, J., & Lassaletta, L. (2013). The nitrogen cascade from agricultural soils to the sea: Modelling nitrogen transfers at regional watershed and global scales. *Philosophical Transactions of the Royal Society B: Biological Sciences*, *368*(1621), 20130123. https://doi.org/10.1098/rstb.2013.0123

Bopp, L., Resplandy, L., Orr, J. C., Doney, S. C., Dunne, J. P., Gehlen, M., Halloran, P., Heinze, C., Ilyina, T., Séférian, R., Tjiputra, J., & Vichi, M. (2013). Multiple stressors of ocean ecosystems in the 21st century: Projections with CMIP5 models. *Biogeosciences*, *10*(10), 6225–6245. https://doi.org/10.5194/bg-10-6225-2013

Boyer, E. W., Howarth, R. W., Galloway, J. N., Dentener, F. J., Green, P. A., Vörösmarty, C. J. (2006). Riverine nitrogen export from the continents to the coasts. *Global Biogeochemical Cycles*, 20(1). doi: https://doi.org/10.1029/2005GB002537

Canadell, J. G., Pedro M.S. Monteiro, Marcos H. Costa, Leticia Cotrim Da Cunha, Peter M. Cox, et al. (2011). Global Carbon and other Biogeochemical Cycles and Feedbacks.

IPCC AR6 WGI, Final Government Distribution, chapter 5. ⟨hal-03336145⟩
Compton, J. E., Harrison, J. A., Dennis, R. L., Greaver, T. L., Hill, B. H., Jordan, S. J., Walker, H., & Campbell, H. V. (2011). Ecosystem services altered by human changes in the nitrogen cycle: A new perspective for US decision making. *Ecology Letters*, *14*(8), 804–815. https://doi.org/10.1111/j.1461-0248.2011.01631.x
Dargie, G. C., Lewis, S. L., Lawson, I. T., Mitchard, E. T. A., Page, S. E., Bocko, Y. E., & Ifo, S. A. (2017). Age, extent and carbon storage of the central Congo Basin peatland complex. *Nature*, *542*(7639), 86–90. https://doi.org/10.1038/nature21048
Denoncourt, C., Chantigny, M. H., Angers, D. A., Maillard, É., & Halde, C. (2025). Animal manure application promotes nitrogen and organic carbon accumulation in soil organic matter fractions: A global meta-analysis. *Science of The Total Environment*, *996*, 180097. https://doi.org/10.1016/j.scitotenv.2025.180097
Diaz, R. J., & Rosenberg, R. (2008). Spreading Dead Zones and Consequences for Marine Ecosystems. *Science*, *321*(5891), 926–929. https://doi.org/10.1126/science.1156401
Drake, P. L., Froend, R. H., & Franks, P. J. (2013). Smaller, faster stomata: Scaling of stomatal size, rate of response, and stomatal conductance. *Journal of Experimental Botany*, *64*(2), 495–505. https://doi.org/10.1093/jxb/ers347
Erisman, J. W., Sutton, M. A., Galloway, J., Klimont, Z., & Winiwarter, W. (2008). How a century of ammonia synthesis changed the world. *Nature Geoscience*, *1*(10), 636–639. https://doi.org/10.1038/ngeo325
Eyring, V., Lamarque, J.-F., Cionni, I., Duncan, B., Fiore, A., Gettelman, A., Hegglin, M., Hess, P., Nagashima, T., Ryerson, T., Shepherd, T. G., Shindell, D. T., Waugh, D., & Young, P. (2013, Jul). IGAC/SPARC Chemistry-Climate Model Initiative (CCMI) 2013 Science Workshop. (50 ed.) International Global Atmospheric Chemistry.
FAO/IIASA/ISRIC/ISSCAS/JRC, A. (2012). *Harmonized World Soil Database (version 1.2)* (Version version 1.2) [Dataset].
Farley, K. A., Jobbágy, E. G., & Jackson, R. B. (2005). Effects of afforestation on water yield: A global synthesis with implications for policy. *Global Change Biology*, *11*(10), 1565–1576. https://doi.org/10.1111/j.1365-2486.2005.01011.x
Federal Institute of Hydrology. (2018). *Global river data centre, Federal Institute of Hydrology, Global Runoff data centre* [Dataset]. https://grdc.bafg.de/data/data_portal/
Feng, M., Peng, S., Wang, Y., Ciais, P., Goll, D. S., Chang, J., Fang, Y., Houlton, B. Z., Liu, G., Sun, Y., & Xi, Y. (2023). Overestimated nitrogen loss from denitrification for natural terrestrial ecosystems in CMIP6 Earth System Models. *Nature Communications*, *14*(1), 3065. https://doi.org/10.1038/s41467-023-38803-z
Fowler, D., Coyle, M., Skiba, U., Sutton, M. A., Cape, J. N., Reis, S., Sheppard, L. J., Jenkins, A., Grizzetti, B., Galloway, J. N., Vitousek, P., Leach, A., Bouwman, A. F., Butterbach-Bahl, K., Dentener, F., Stevenson, D., Amann, M., & Voss, M. (2013). The global nitrogen cycle in the twenty-first century. *Philosophical Transactions of the Royal Society B: Biological Sciences*, *368*(1621), 20130164. https://doi.org/10.1098/rstb.2013.0164
Galloway, J. N. (2003). 8.12—The Global Nitrogen Cycle. In H. D. Holland & K. K. Turekian (Eds.), *Treatise on Geochemistry* (pp. 557–583). Pergamon. https://doi.org/10.1016/B0-08-043751-6/08160-3
Gao, W., Yang, H., Kou, L., & Li, S. (2015). Effects of nitrogen deposition and fertilization on N transformations in forest soils: A review. *Journal of Soils and Sediments*, *15*(4), 863–879. https://doi.org/10.1007/s11368-015-1064-z
Goll, D. S., Joetzjer, E., Huang, M., & Ciais, P. (2018). Low Phosphorus Availability Decreases Susceptibility of Tropical Primary Productivity to Droughts. *Geophysical Research Letters*, *45*(16), 8231–8240. https://doi.org/10.1029/2018GL077736

Goll, D. S., Vuichard, N., Maignan, F., Jornet-Puig, A., Sardans, J., Violette, A., Peng, S., Sun, Y., Kvakic, M., Guimberteau, M., Guenet, B., Zaehle, S., Penuelas, J., Janssens, I., & Ciais, P. (2017). A representation of the phosphorus cycle for ORCHIDEE (revision 4520). *Geoscientific Model Development*, *10*(10), 3745–3770. https://doi.org/10.5194/gmd-10-3745-2017

Gordon, B. A., Dorothy, O., & Lenhart, C. F. (2020). Nutrient Retention in Ecologically Functional Floodplains: A Review. *Water*, *12*(10). https://doi.org/10.3390/w12102762

Green, P. A., Vörösmarty, C. J., Meybeck, M., Galloway, J. N., Peterson, B. J., Boyer, E. W. (2004). Pre-industrial and contemporary fluxes of nitrogen through rivers: a global assessment based on typology. *Biogeochemistry*, 68(1):71-105. doi:10.1023/B:BIOG.0000025742.82155.92

Gruber, N., & Galloway, J. N. (2008). An Earth-system perspective of the global nitrogen cycle. *Nature*, *451*(7176), 293–296. https://doi.org/10.1038/nature06592

Gu, X., Wang, Y., Laanbroek, H. J., Xu, X., Song, B., Huo, Y., Chen, S., Li, L., & Zhang, L. (2019). Saturated N2O emission rates occur above the nitrogen deposition level predicted for the semi-arid grasslands of Inner Mongolia, China. *Geoderma*, *341*, 18–25. https://doi.org/10.1016/j.geoderma.2019.01.002

Guimberteau, M., Drapeau, G., Ronchail, J., Sultan, B., Polcher, J., Martinez, J.-M., Prigent, C., Guyot, J.-L., Cochonneau, G., Espinoza, J. C., Filizola, N., Fraizy, P., Lavado, W., De Oliveira, E., Pombosa, R., Noriega, L., & Vauchel, P. (2012). Discharge simulation in the sub-basins of the Amazon using ORCHIDEE forced by new datasets. *Hydrology and Earth System Sciences*, *16*(3), 911–935. https://doi.org/10.5194/hess-16-911-2012

Hagedorn, F., van Hees, P. A. W., Handa, I. T., & Hättenschwiler, S. (2008). Elevated atmospheric CO2 fuels leaching of old dissolved organic matter at the alpine treeline. *Global Biogeochemical Cycles*, *22*(2). https://doi.org/10.1029/2007GB003026

Harris, I., Jones, P. D., Osborn, T. J., & Lister, D. H. (2014). Updated high-resolution grids of monthly climatic observations – the CRU TS3.10 Dataset. *International Journal of Climatology*, *34*(3), 623–642. https://doi.org/10.1002/joc.3711

Harrison, J.A., Maranger, R.J., Alexander, R.B. et al. (2009). The regional and global significance of nitrogen removal in lakes and reservoirs. *Biogeochemistry*, 93, 143–157. https://doi.org/10.1007/s10533-008-9272-x

Hu, M., Chen, D., & Dahlgren, R. A. (2016). Modeling nitrous oxide emission from rivers: A global assessment. *Global Change Biology*, *22*(11), 3566–3582. https://doi.org/10.1111/gcb.13351

Hurtt, G. C., Chini, L., Sahajpal, R., Frolking, S., Bodirsky, B. L., Calvin, K., Doelman, J. C., Fisk, J., Fujimori, S., Klein Goldewijk, K., Hasegawa, T., Havlik, P., Heinimann, A., Humpenöder, F., Jungclaus, J., Kaplan, J. O., Kennedy, J., Krisztin, T., Lawrence, D., … Zhang, X. (2020). Harmonization of global land use change and management for the period 850–2100 (LUH2) for CMIP6. *Geoscientific Model Development*, *13*(11), 5425–5464. https://doi.org/10.5194/gmd-13-5425-2020

Johnson, D. W., Cheng, W., Joslin, J. D., Norby, R. J., Edwards, N. T., & Todd, D. E. (2004). Effects of elevated CO2 on nutrient cycling in a sweetgum plantation. *Biogeochemistry*, *69*(3), 379–403. https://doi.org/10.1023/B:BIOG.0000031054.19158.7c

Kannel, P. R., Lee, S., Lee, Y.-S., Kanel, S. R., & Pelletier, G. J. (2007). Application of automated QUAL2Kw for water quality modeling and management in the Bagmati River, Nepal. *Ecological Modelling*, *202*(3), 503–517. https://doi.org/10.1016/j.ecolmodel.2006.12.033

Kemp, M. J., & Dodds, W. K. (2002). The influence of ammonium, nitrate, and dissolved oxygen concentrations on uptake, nitrification, and denitrification rates associated with prairie stream substrata. *Limnology and Oceanography*, *47*(5), 1380–1393. https://doi.org/10.4319/lo.2002.47.5.1380

Koenig, L. E., Song, C., Wollheim, W. M., Rüegg, J., & McDowell, W. H. (2017). Nitrification increases nitrogen export from a tropical river network. *Freshwater Science*, *36*(4), 698–712. https://doi.org/10.1086/694906

Krinner, G., Viovy, N., de Noblet-Ducoudré, N., Ogée, J., Polcher, J., Friedlingstein, P., Ciais, P., Sitch, S., & Prentice, I. C. (2005). A dynamic global vegetation model for studies of the coupled atmosphere-biosphere system. *Global Biogeochemical Cycles*, *19*(1). https://doi.org/10.1029/2003GB002199

Kroeze, C., Mosier, A., and Bouwman, L. (1999), Closing the global N_2O budget: A retrospective analysis 1500–1994, *Global Biogeochem. Cycles*, 13(1), 1–8, doi:10.1029/1998GB900020

Kroeze, C., Dumont, E., & Seitzinger, S. P. (2005). New estimates of global emissions of N2O from rivers and estuaries. *Environmental Sciences*, *2*(2–3), 159–165. https://doi.org/10.1080/15693430500384671

Laini, A., Bartoli, M., Castaldi, S., Viaroli, P., Capri, E., & Trevisan, M. (2011). Greenhouse gases (CO2, CH4 and N2O) in lowland springs within an agricultural impacted watershed (Po River Plain, northern Italy). *Chemistry and Ecology*, *27*(2), 177–187. https://doi.org/10.1080/02757540.2010.547489

Lamarque, J.-F., Dentener, F., McConnell, J., Ro, C.-U., Shaw, M., Vet, R., Bergmann, D., Cameron-Smith, P., Dalsoren, S., Doherty, R., Faluvegi, G., Ghan, S. J., Josse, B., Lee, Y. H., MacKenzie, I. A., Plummer, D., Shindell, D. T., Skeie, R. B., Stevenson, D. S., … Nolan, M. (2013). Multi-model mean nitrogen and sulfur deposition from the Atmospheric Chemistry and Climate Model Intercomparison Project (ACCMIP): Evaluation of historical and projected future changes. *Atmospheric Chemistry and Physics*, *13*(16), 7997–8018. https://doi.org/10.5194/acp-13-7997-2013

Lauerwald, R., Regnier, P., Figueiredo, V., Enrich-Prast, A., Bastviken, D., Lehner, B., Maavara, T., Raymond, P. (2019). Natural lakes are a minor global source of N2O to the atmosphere. Global Biogeochemical Cycles, 33, 1564–1581. https://doi.org/10.1029/2019GB006261

Le Quéré, C., Andrew, R. M., Friedlingstein, P., Sitch, S., Pongratz, J., Manning, A. C., Korsbakken, J. I., Peters, G. P., Canadell, J. G., Jackson, R. B., Boden, T. A., Tans, P. P., Andrews, O. D., Arora, V. K., Bakker, D. C. E., Barbero, L., Becker, M., Betts, R. A., Bopp, L., … Zhu, D. (2018). Global Carbon Budget 2017. *Earth System Science Data*, *10*(1), 405–448. https://doi.org/10.5194/essd-10-405-2018

LeBauer, D. S., & Treseder, K. K. (2008). NITROGEN LIMITATION OF NET PRIMARY PRODUCTIVITY IN TERRESTRIAL ECOSYSTEMS IS GLOBALLY DISTRIBUTED. *Ecology*, *89*(2), 371–379. https://doi.org/10.1890/06-2057.1

Lee, M., Shevliakova, E., Stock, C. A., Malyshev, S., & Milly, P. C. D. (2019). Prominence of the tropics in the recent rise of global nitrogen pollution. *Nature Communications*, *10*(1), 1437. https://doi.org/10.1038/s41467-019-09468-4

Li, C., Aber, J., Stange, F., Butterbach-Bahl, K., & Papen, H. (2000). A process-oriented model of N2O and NO emissions from forest soils: 1. Model development. *Journal of Geophysical Research: Atmospheres*, *105*(D4), 4369–4384. https://doi.org/10.1029/1999JD900949

Li, C., Frolking, S., & Frolking, T. A. (1992). A model of nitrous oxide evolution from soil driven by rainfall events: 1. Model structure and sensitivity. *Journal of Geophysical Research: Atmospheres*, *97*(D9), 9759–9776. https://doi.org/10.1029/92JD00509

Li, X., Sardans, J., Qi, M., Ni, X., Zhang, M., Peñuelas, J., Yue, K., & Wu, F. (2022). Nitrous oxide concentration and flux in Min River Basin of southeast China: Effects of land use, stream order and water variables. *Journal of Hydrology*, *614*, 128507. https://doi.org/10.1016/j.jhydrol.2022.128507

Liu, M., Raymond, P.A., Lauerwald, R. et al. (2024) Global riverine land-to-ocean carbon export constrained by observations and multi-model assessment. Nat. Geosci. 17, 896–904. https://doi.org/10.1038/s41561-024-01524-z

Liu, S., Lu, D., Painter, S. L., Griffiths, N. A., & Pierce, E. M. (2023). Uncertainty quantification of machine learning models to improve streamflow prediction under changing climate and environmental conditions. *Frontiers in Water*, *Volume 5-2023*. https://doi.org/10.3389/frwa.2023.1150126

Lu, C., & Tian, H. (2017). Global nitrogen and phosphorus fertilizer use for agriculture production in the past half century: Shifted hot spots and nutrient imbalance. *Earth System Science Data*, *9*(1), 181–192. https://doi.org/10.5194/essd-9-181-2017

Luek, J. L., Brooker, M. R., Ash, B. L., Midden, W. R., & Mouser, P. J. (2020). Seasonal changes predominant over manure application in driving dissolved organic matter shifts in agricultural runoff. *Journal of Great Lakes Research*, *46*(6), 1570–1580. https://doi.org/10.1016/j.jglr.2020.09.017

Lurton, T., Balkanski, Y., Bastrikov, V., Bekki, S., Bopp, L., Braconnot, P., Brockmann, P., Cadule, P., Contoux, C., Cozic, A., Cugnet, D., Dufresne, J.-L., Éthé, C., Foujols, M.-A., Ghattas, J., Hauglustaine, D., Hu, R.-M., Kageyama, M., Khodri, M., … Boucher, O. (2020). Implementation of the CMIP6 Forcing Data in the IPSL-CM6A-LR Model. *Journal of Advances in Modeling Earth Systems*, *12*(4), e2019MS001940. https://doi.org/10.1029/2019MS001940

Lutz, B. D., Bernhardt, E. S., Roberts, B. J., & Mulholland, P. J. (2011). Examining the coupling of carbon and nitrogen cycles in Appalachian streams: The role of dissolved organic nitrogen. *Ecology*, *92*(3), 720–732. https://doi.org/10.1890/10-0899.1

Ma, M., Song, C., Fang, H., Zhang, J., Wei, J., Liu, S., Chen, X., Zhang, K., Yuan, W., & Lu, H. (2022). Development of a Process-Based N2O Emission Model for Natural Forest and Grassland Ecosystems. *Journal of Advances in Modeling Earth Systems*, *14*(3), e2021MS002460. https://doi.org/10.1029/2021MS002460

Ma, M., Zhang, H., Lauerwald, R., Ciais, P., & Regnier, P. (2025). Estimating lateral nitrogen transfers over the last century through the global river network using a land surface model. *Earth System Dynamics*, *16*(3), 841–867. https://doi.org/10.5194/esd-16-841-2025

Maavara, T., Lauerwald, R., Laruelle, G. G., Akbarzadeh, Z., Bouskill, N. J., Van Cappellen, P., & Regnier, P. (2019). Nitrous oxide emissions from inland waters: Are IPCC estimates too high? *Global Change Biology*, *25*(2), 473–488. https://doi.org/10.1111/gcb.14504

Maranger, R., Jones, S. E., & Cotner, J. B. (2018). Stoichiometry of carbon, nitrogen, and phosphorus through the freshwater pipe. *Limnology and Oceanography Letters*, *3*(3), 89–101. https://doi.org/10.1002/lol2.10080

Martinez-Rey, J., Bopp, L., Gehlen, M., Tagliabue, A., & Gruber, N. (2015). Projections of oceanic N_2O emissions in the 21st century using the IPSL Earth system model. *Biogeosciences*, *12*(13), 4133–4148. https://doi.org/10.5194/bg-12-4133-2015

Marzadri, A., Amatulli, G., Tonina, D., Bellin, A., Shen, L. Q., Allen, G. H., & Raymond, P. A. (2021). Global riverine nitrous oxide emissions: The role of small streams and large rivers. *Science of The Total Environment*, *776*, 145148. https://doi.org/10.1016/j.scitotenv.2021.145148

Marzadri, A., Bellin, A., Tank, J. L., & Tonina, D. (2022). Predicting nitrous oxide emissions through riverine networks. *Science of The Total Environment*, *843*, 156844. https://doi.org/10.1016/j.scitotenv.2022.156844

Mayer, P. M., Reynolds Jr., S. K., McCutchen, M. D., & Canfield, T. J. (2007). Meta-Analysis of Nitrogen Removal in Riparian Buffers. *Journal of Environmental Quality*, *36*(4), 1172–1180. https://doi.org/10.2134/jeq2006.0462

Mayorga, E., Seitzinger, S. P., Harrison, J. A., Dumont, E., Beusen, A. H. W., Bouwman, A. F., Fekete, B. M., Kroeze, C., & Drecht, G. V. (2010). Global Nutrient Export from WaterSheds 2 (NEWS 2): Model development and implementation. *Environmental Modelling & Software*, *25*(7), 837–853. https://doi.org/10.1016/j.envsoft.2010.01.007

McClelland, J. W., Holmes, R. M., Dunton, K. H., & Macdonald, R. W. (2012). The Arctic Ocean Estuary. *Estuaries and Coasts*, *35*(2), 353–368. https://doi.org/10.1007/s12237-010-9357-3

McCutcheon, S. (1987). Laboratory and Instream Nitrification Rates for Selected Streams. *Journal of Environmental Engineering*, *113*(3), 628–646. https://doi.org/10.1061/(ASCE)0733-9372(1987)113:3(628)

McDowell, W. H., Magill, A. H., Aitkenhead-Peterson, J. A., Aber, J. D., Merriam, J. L., & Kaushal, S. S. (2004). Effects of chronic nitrogen amendment on dissolved organic matter and inorganic nitrogen in soil solution. *Forest Ecology and Management*, *196*(1), 29–41. https://doi.org/10.1016/j.foreco.2004.03.010

Morée, A. L., Beusen, A. H. W., Bouwman, A. F., & Willems, W. J. (2013). Exploring global nitrogen and phosphorus flows in urban wastes during the twentieth century. *Global Biogeochemical Cycles*, *27*(3), 836–846. https://doi.org/10.1002/gbc.20072

Naden, P., Bell, V., Carnell, E., Tomlinson, S., Dragosits, U., Chaplow, J., May, L., & Tipping, E. (2016). Nutrient fluxes from domestic wastewater: A national-scale historical perspective for the UK 1800–2010. *Science of The Total Environment*, *572*, 1471–1484. https://doi.org/10.1016/j.scitotenv.2016.02.037

Nakhavali, M. (Andre), Lauerwald, R., Regnier, P., & Friedlingstein, P. (2024). Historical trends and drivers of the laterally transported terrestrial dissolved organic carbon to river systems. *Science of The Total Environment*, *917*, 170560. https://doi.org/10.1016/j.scitotenv.2024.170560

Niklaus, P. A., Kandeler, E., Leadley, P. W., Schmid, B., Tscherko, D., & Körner, C. (2001). A link between plant diversity, elevated CO2 and soil nitrate. *Oecologia*, *127*(4), 540–548. https://doi.org/10.1007/s004420000612

Noe, G. B., & Hupp, C. R. (2005). CARBON, NITROGEN, AND PHOSPHORUS ACCUMULATION IN FLOODPLAINS OF ATLANTIC COASTAL PLAIN RIVERS, USA. *Ecological Applications*, *15*(4), 1178–1190. https://doi.org/10.1890/04-1677

Pauer, J. J., & Auer, M. T. (2009). Formulation and testing of a novel river nitrification model. *Ecological Modelling*, *220*(6), 857–866. https://doi.org/10.1016/j.ecolmodel.2008.12.014

Pelletier, G., & Chapra, S. (2006). *A modeling framework for simulating river and stream water quality* (pp. 98504–97710) [Environmental Assessment Program].

Raimonet, M., Cazier, T., Rocher, V., & Laverman, A. M. (2017). Nitrifying Kinetics and the Persistence of Nitrite in the Seine River, France. *Journal of Environmental Quality*, *46*(3), 585–595. https://doi.org/10.2134/jeq2016.06.0242

Ravishankara, A. R., Daniel, J. S., & Portmann, R. W. (2009). Nitrous Oxide (N_2O): The Dominant Ozone-Depleting Substance Emitted in the 21st Century. *Science*, *326*(5949), 123–125. https://doi.org/10.1126/science.1176985

Regnier, P., Friedlingstein, P., Ciais, P., Mackenzie, F. T., Gruber, N., Janssens, I. A., Laruelle, G. G., Lauerwald, R., Luyssaert, S., Andersson, A. J., Arndt, S., Arnosti, C., Borges, A. V., Dale, A. W., Gallego-Sala, A., Goddéris, Y., Goossens, N., Hartmann, J., Heinze, C., Thullner, M. (2013). Anthropogenic perturbation of the carbon fluxes from land to ocean. *Nature Geoscience*, *6*(8), 597–607. https://doi.org/10.1038/ngeo1830

Regnier, P., Resplandy, L., Najjar, R. G., & Ciais, P. (2022). The land-to-ocean loops of the global carbon cycle. *Nature*, *603*(7901), 401–410. https://doi.org/10.1038/s41586-021-04339-9

Reynolds, C., Jackson, T., & Rawls, W. (1999). Estimating available water content by linking the FAO soil map of the world with global soil profile databases and pedo-transfer functions. *Transactions*, *80*(S132).

Rodríguez-Cardona, B. M., Wymore, A. S., Argerich, A., Barnes, R. T., Bernal, S., Brookshire, E. N. J., Coble, A. A., Dodds, W. K., Fazekas, H. M., Helton, A. M., Johnes, P. J., Johnson, S. L., Jones, J. B., Kaushal, S. S., Kortelainen, P., López-Lloreda, C., Spencer, R. G. M., & McDowell, W. H. (2022). Shifting stoichiometry: Long-term trends in stream-dissolved organic matter reveal altered C:N ratios due to history of atmospheric acid deposition. *Global Change Biology*, *28*(1), 98–114. https://doi.org/10.1111/gcb.15965

Roley, S. S., Tank, J. L., Stephen, M. L., Johnson, L. T., Beaulieu, J. J., & Witter, J. D. (2012). Floodplain restoration enhances denitrification and reach-scale nitrogen removal in an agricultural stream. *Ecological Applications*, *22*(1), 281–297. https://doi.org/10.1890/11-0381.1

Saunders, D., Kalff, J. (2001). Nitrogen retention in wetlands, lakes and rivers. *Hydrobiologia*, 443, 205–212 (2001). https://doi.org/10.1023/A:1017506914063

Schmadel, N. M., Harvey, J. W., Alexander, R. B., Schwarz, G. E., Moore, R. B., Eng, K., Gomez-Velez, J. D., Boyer, E. W., & Scott, D. (2018). Thresholds of lake and reservoir connectivity in river networks control nitrogen removal. *Nature Communications*, *9*(1), 2779. https://doi.org/10.1038/s41467-018-05156-x

Shcherbak, I., Millar, N., Robertson, G. P. (2014) Global metaanalysis of the nonlinear response of soil nitrous oxide (N_2O) emissions to fertilizer nitrogen. Proc Natl Acad Sci U S A, 111(25):9199-204. doi: 10.1073/pnas.1322434111

Schulz, G., Sanders, T., Voynova, Y. G., Bange, H. W., & Dähnke, K. (2023). Seasonal variability of nitrous oxide concentrations and emissions in a temperate estuary. Biogeosciences, 20(15), 3229–3247. https://doi.org/10.5194/bg-20-3229-2023

Seiler, C., Kou-Giesbrecht, S., Arora, V. K., & Melton, J. R. (2024). The Impact of Climate Forcing Biases and the Nitrogen Cycle on Land Carbon Balance Projections. *Journal of Advances in Modeling Earth Systems*, *16*(1), e2023MS003749. https://doi.org/10.1029/2023MS003749

Seitzinger, S., Harrison, J. A., Böhlke, J. K., Bouwman, A. F., Lowrance, R., Peterson, B., Tobias, C., & Drecht, G. V. (2006). DENITRIFICATION ACROSS LANDSCAPES AND WATERSCAPES: A SYNTHESIS. *Ecological Applications*, *16*(6), 2064–2090. https://doi.org/10.1890/1051-0761(2006)016%5B2064:DALAWA%5D2.0.CO;2

Seitzinger, S. P., Harrison, J. A., Dumont, E., Beusen, A. H. W., & Bouwman, A. F. (2005). Sources and delivery of carbon, nitrogen, and phosphorus to the coastal zone: An overview of Global Nutrient Export from Watersheds (NEWS) models and their application. *Global Biogeochemical Cycles*, *19*(4). https://doi.org/10.1029/2005GB002606

Seitzinger, S. P., Mayorga, E., Bouwman, A. F., Kroeze, C., Beusen, A. H. W., Billen, G., Van Drecht, G., Dumont, E., Fekete, B. M., Garnier, J., & Harrison, J. A. (2010).

Global river nutrient export: A scenario analysis of past and future trends. *Global Biogeochemical Cycles*, *24*(4). https://doi.org/10.1029/2009GB003587

Shammas, N. Kh. (1986). Interactions of Temperature, pH, and Biomass on the Nitrification Process. *Journal (Water Pollution Control Federation)*, *58*(1), 52–59. JSTOR. https://www.jstor.org/stable/25042841

Shen, L. Q., Amatulli, G., Sethi, T., Raymond, P., & Domisch, S. (2020). Estimating nitrogen and phosphorus concentrations in streams and rivers, within a machine learning framework. *Scientific Data*, *7*(1), 161. https://doi.org/10.1038/s41597-020-0478-7

Sun, Y., Goll, D. S., Chang, J., Ciais, P., Guenet, B., Helfenstein, J., Huang, Y., Lauerwald, R., Maignan, F., Naipal, V., Wang, Y., Yang, H., & Zhang, H. (2021). Global evaluation of the nutrient-enabled version of the land surface model ORCHIDEE-CNP v1.2 (r5986). *Geoscientific Model Development*, *14*(4), 1987–2010. https://doi.org/10.5194/gmd-14-1987-2021

Takeda, N., Friedl, J., Rowlings, D., Rosa, D. D., Scheer, C., Grace, P. (2021). Exponential response of nitrous oxide (N_2O) emissions to increasing nitrogen fertiliser rates in a tropical sugarcane cropping system. Agriculture, Ecosystems & Environment, 313:107376. doi: https://doi.org/10.1016/j.agee.2021.107376

Terrer, C., Jackson, R. B., Prentice, I. C., Keenan, T. F., Kaiser, C., Vicca, S., Fisher, J. B., Reich, P. B., Stocker, B. D., Hungate, B. A., Peñuelas, J., McCallum, I., Soudzilovskaia, N. A., Cernusak, L. A., Talhelm, A. F., Van Sundert, K., Piao, S., Newton, P. C. D., Hovenden, M. J., … Franklin, O. (2019). Nitrogen and phosphorus constrain the CO2 fertilization of global plant biomass. *Nature Climate Change*, *9*(9), 684–689. https://doi.org/10.1038/s41558-019-0545-2

Thornton, P. E., Lamarque, J.-F., Rosenbloom, N. A., & Mahowald, N. M. (2007). Influence of carbon-nitrogen cycle coupling on land model response to CO2 fertilization and climate variability. *Global Biogeochemical Cycles*, *21*(4). https://doi.org/10.1029/2006GB002868

Tian, H., Bian, Z., Shi, H., Qin, X., Pan, N., Lu, C., Pan, S., Tubiello, F. N., Chang, J., Conchedda, G., Liu, J., Mueller, N., Nishina, K., Xu, R., Yang, J., You, L., & Zhang, B. (2022). History of anthropogenic Nitrogen inputs (HaNi) to the terrestrial biosphere: A 5 arcmin resolution annual dataset from 1860 to 2019. *Earth System Science Data*, *14*(10), 4551–4568. https://doi.org/10.5194/essd-14-4551-2022

Tian, H., Yang, J., Lu, C., Xu, R., Canadell, J. G., Jackson, R. B., Arneth, A., Chang, J., Chen, G., Ciais, P., Gerber, S., Ito, A., Huang, Y., Joos, F., Lienert, S., Messina, P., Olin, S., Pan, S., Peng, C., Zhu, Q. (2018). The Global N_2O Model Intercomparison Project. *Bulletin of the American Meteorological Society*, *99*(6), 1231–1251. https://doi.org/10.1175/BAMS-D-17-0212.1

Tipping, E., Somerville, C. J., & Luster, J. (2016). The C:N:P:S stoichiometry of soil organic matter. *Biogeochemistry*, *130*(1), 117–131. https://doi.org/10.1007/s10533-016-0247-z

Tian H., Pan N., Thompson R. L., et al. (2024). Global nitrous oxide budget (1980–2020). *Earth System Science Data*, 16(6):2543-2604. doi:10.5194/essd-16-2543-2024

Tivig, M., Keller, D.P., Oschlies A. (2021). Riverine nitrogen supply to the global ocean and its limited impact on global marine primary production: a feedback study using an Earth system model. *Biogeosciences*, 18(19):5327-5350. doi:10.5194/bg-18-5327-2021

Tschikof, M., Gericke, A., Venohr, M., Weigelhofer, G., Bondar-Kunze, E., Kaden, U. S., & Hein, T. (2022). The potential of large floodplains to remove nitrate in river basins – The Danube case. *Science of The Total Environment*, *843*, 156879. https://doi.org/10.1016/j.scitotenv.2022.156879

Upadhyay, P., Prajapati, S. K., & Kumar, A. (2026). Spatiotemporal Variability and Underlying Drivers of Greenhouse Gas Emissions from the Subtropical Ganga River Network, India. *ACS ES&T Water*, *6*(1), 240–253. https://doi.org/10.1021/acsestwater.5c00967

Vilmin, L., Mogollón, J. M., Beusen, A. H. W., & Bouwman, A. F. (2018). Forms and subannual variability of nitrogen and phosphorus loading to global river networks over the 20th century. *Global and Planetary Change*, *163*, 67–85. https://doi.org/10.1016/j.gloplacha.2018.02.007

Virro, H., Amatulli, G., Kmoch, A., Shen, L., & Uuemaa, E. (2021). GRQA: Global River Water Quality Archive. *Earth System Science Data*, *13*(12), 5483–5507. https://doi.org/10.5194/essd-13-5483-2021

Vörösmarty, C. J., Fekete, B. M., Meybeck, M., & Lammers, R. B. (2000). Geomorphometric attributes of the global system of rivers at 30-minute spatial resolution. *Journal of Hydrology*, *237*(1), 17–39. https://doi.org/10.1016/S0022-1694(00)00282-1

Vuichard, N., Messina, P., Luyssaert, S., Guenet, B., Zaehle, S., Ghattas, J., Bastrikov, V., & Peylin, P. (2019). Accounting for carbon and nitrogen interactions in the global terrestrial ecosystem model ORCHIDEE (trunk version, rev 4999): Multi-scale evaluation of gross primary production. *Geoscientific Model Development*, *12*(11), 4751–4779. https://doi.org/10.5194/gmd-12-4751-2019

Wang, J., Vilmin, L., Mogollón, J. M., Beusen, A. H. W., van Hoek, W. J., Liu, X., Pika, P. A., Middelburg, J. J., & Bouwman, A. F. (2023). Inland Waters Increasingly Produce and Emit Nitrous Oxide. *Environmental Science & Technology*, *57*(36), 13506–13519. https://doi.org/10.1021/acs.est.3c04230

Wang, Z., Wang, H., Wang, T., Wang, L., Liu, X., Zheng, K., & Huang, X. (2022). Large discrepancies of global greening: Indication of multi-source remote sensing data. *Global Ecology and Conservation*, *34*, e02016. https://doi.org/10.1016/j.gecco.2022.e02016

Wang S., Lan B., Yu L., Xiao M., Jiang L., Qin, Y., Jin, Y., Zhou, Y., Armanbek, G., Ma, J., Wang, M., Jetten, M. S. M., Tian, H., Zhu, G., Zhu, Y. G. (2024). Ammonium-derived nitrous oxide is a global source in streams. *Nat Commun*, 14, 15(1):4085. doi: https://doi.org/10.1038/s41467-024-48343-9

Wellen, C., Kamean-Disfani, A. R., & Arhonditsis, G. B. (2015). Evaluation of the current state of distributed watershed nutrient water quality modeling. *Environ Sci Technol*, *17*(49(6)), 3278–3290. https://doi.org/10.1021/es5049557

Wollheim, W. M., Vörösmarty, C. J., Bouwman, A. F., Green, P., Harrison, J., Linder, E., Peterson, B. J., Seitzinger, S. P., & Syvitski, J. P. M. (2008). Global N removal by freshwater aquatic systems using a spatially distributed, within-basin approach. *Global Biogeochemical Cycles*, *22*(2). https://doi.org/10.1029/2007GB002963

Wright, S. J., Turner, B. L., Yavitt, J. B., Harms, K. E., Kaspari, M., Tanner, E. V. J., Bujan, J., Griffin, E. A., Mayor, J. R., Pasquini, S. C., Sheldrake, M., & Garcia, M. N. (2018). Plant responses to fertilization experiments in lowland, species-rich, tropical forests. *Ecology*, *99*(5), 1129–1138. https://doi.org/10.1002/ecy.2193

Wu, J., Wang, H., & Li, G. (2023). Effects of nitrogen deposition on N2O emission in a wet meadow on the Qinghai-Tibet Plateau. *Applied Soil Ecology*, *191*, 105049. https://doi.org/10.1016/j.apsoil.2023.105049

Wymore, A. S., Johnes, P. J., Bernal, S., Brookshire, E. N. J., Fazekas, H. M., Helton, A. M., Argerich, A., Barnes, R. T., Coble, A. A., Dodds, W. K., Haq, S., Johnson, S. L., Jones, J. B., Kaushal, S. S., Kortelainen, P., López-Lloreda, C., Rodríguez-Cardona, B. M., Spencer, R. G. M., Sullivan, P. L., … McDowell, W. H. (2021). Gradients of Anthropogenic Nutrient Enrichment Alter N Composition and DOM Stoichiometry in

Freshwater Ecosystems. *Global Biogeochemical Cycles*, *35*(8), e2021GB006953. https://doi.org/10.1029/2021GB006953

Yang, Q., Tian, H., Friedrichs, M. A. M., Hopkinson, C. S., Lu, C., & Najjar, R. G. (2015). Increased nitrogen export from eastern North America to the Atlantic Ocean due to climatic and anthropogenic changes during 1901–2008. *Journal of Geophysical Research Biogeosciences*, *120*(6), 1046–1068. https://doi.org/10.1002/2014JG002763

Yao, Y., Tian, H., Shi, H., Pan, S., Xu, R., Pan, N., & Canadell, J. G. (2020). Increased global nitrous oxide emissions from streams and rivers in the Anthropocene. *Nature Climate Change*, *10*(2), 138–142. https://doi.org/10.1038/s41558-019-0665-8

Zaehle, S. (2013). Terrestrial nitrogen–carbon cycle interactions at the global scale. *Philos Trans R Soc Lond B Biol Sci*, *368*(1621). https://doi.org/10.1098/rstb.2013.0125

Zaehle, S., & Friend, A. D. (2010). Carbon and nitrogen cycle dynamics in the O-CN land surface model: 1. Model description, site-scale evaluation, and sensitivity to parameter estimates. *Global Biogeochemical Cycles*, *24*(1). https://doi.org/10.1029/2009GB003521

Zaehle, S., Medlyn, B. E., De Kauwe, M. G., et a. (2014). Evaluation of 11 terrestrial carbon–nitrogen cycle models against observations from two temperate Free-Air CO2 Enrichment studies. *New Phytologist*, *202*(3), 803–822. https://doi.org/10.1111/nph.12697

Zhang, H., Lauerwald, R., Ciais, P., Van Oost, K., Guenet, B., & Regnier, P. (2022). Global changes alter the amount and composition of land carbon deliveries to European rivers and seas. *Communications Earth & Environment*, *3*(1), 245. https://doi.org/10.1038/s43247-022-00575-7

Zhang, H., Lauerwald, R., Regnier, P., Ciais, P., Van Oost, K., Naipal, V., Guenet, B., & Yuan, W. (2022). Estimating the lateral transfer of organic carbon through the European river network using a land surface model. *Earth System Dynamics*, *13*(3), 1119–1144. https://doi.org/10.5194/esd-13-1119-2022

Zhang, H., Lauerwald, R., Regnier, P., Ciais, P., Yuan, W., Naipal, V., Guenet, B., Van Oost, K., & Camino-Serrano, M. (2020). Simulating Erosion-Induced Soil and Carbon Delivery From Uplands to Rivers in a Global Land Surface Model. *Journal of Advances in Modeling Earth Systems*, *12*(11), e2020MS002121. https://doi.org/10.1029/2020MS002121

Zhang, Y., Li, C., Trettin, C. C., Li, H., & Sun, G. (2002). An integrated model of soil, hydrology, and vegetation for carbon dynamics in wetland ecosystems. *Global Biogeochemical Cycles*, *16*(4), 9-1-9–17. https://doi.org/10.1029/2001GB001838

Zheng, Z.-Z., Wan, X., Xu, M. N., Hsiao, S. S.-Y., Zhang, Y., Zheng, L.-W., Wu, Y., Zou, W., & Kao, S.-J. (2017). Effects of temperature and particles on nitrification in a eutrophic coastal bay in southern China. *Journal of Geophysical Research: Biogeosciences*, *122*(9), 2325–2337. https://doi.org/10.1002/2017JG003871

Zhu, D., Cheng, X., Sample, D. J., Qiao, Q., & Liu, Z. (2023). Effect of water temperature on internal nitrogen release from sediments in the Pearl River Delta region, China. *Hydrology Research*, *54*(9), 1055–1071. https://doi.org/10.2166/nh.2023.056

Zhu, J., Jia, Y., Yu, G., Wang, Q., He, N., Chen, Z., He, H., Zhu, X., Li, P., Zhang, F., Liu, X., Goulding, K., Fowler, D., & Vitousek, P. (2025). Changing patterns of global nitrogen deposition driven by socio-economic development. *Nature Communications*, *16*(1), 46. https://doi.org/10.1038/s41467-024-55606-y

Zuijdgeest, A. L., Zurbrügg, R., Blank, N., Fulcri, R., Senn, D. B., & Wehrli, B. (2015). Seasonal dynamics of carbon and nutrients from two contrasting tropical floodplain systems in the Zambezi River basin. *Biogeosciences*, *12*(24), 7535–7547. https://doi.org/10.5194/bg-12-7535-2015